Inorganic Chemistry

Article

pubs.acs.org/IC

Systematic Investigation of Relationship between Strength of NH···S Hydrogen Bond and Reactivity of Molybdoenzyme Models

Taka-aki Okamura,* Yasuhito Ushijima, Yui Omi, and Kiyotaka Onitsuka

Department of Macromolecular Science, Graduate School of Science, Osaka University, Toyonaka, Osaka 560-0043, Japan

Supporting Information

ABSTRACT: A series of monooxomolybdenum(IV) and dioxomolybdenum(VI) complexes containing two intramolecular NH···S hydrogen bonds were synthesized and characterized by ^{1}H NMR, UV−visible, IR, and Raman spectroscopies, and electrochemical measurements. Elimination of the steric effects enabled the accurate and quantitative evaluation of NH···S hydrogen bonds. Strong correlations among the strength of the hydrogen bond, the strength of the Mo^{VI}═O bond, and the redox potential were clearly shown. The hydrogen bonds stabilize the intermediate in the reaction between the monooxomolybdenum(IV) and Me_3NO, resulting in acceleration of the reaction or retardation of *trans*−*cis* rearrangement. The proposed intermediate and the reaction mechanism, discussed on the basis of theoretical calculations, provided a unified explanation of the reaction.

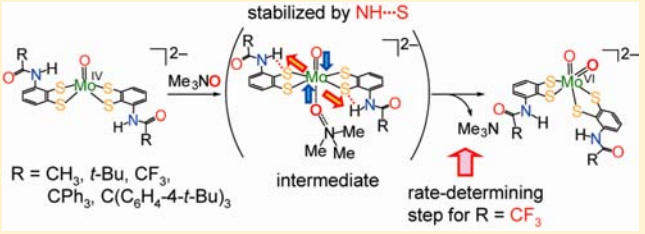

INTRODUCTION

The dimethyl sulfoxide reductase (DMSOR) family of molybdenum enzymes, which contains two molybdopterins, catalyzes oxygen atom transfer reactions between water and substrates using Mo^{IV} and Mo^{VI} oxidation states, with some exceptions.[1,2] DMSOR and trimethylamine-*N*-oxide reductase (TMAOR) reduce Me_3NO to Me_3N, which results in the formation of a Mo^{VI}═O bond.[1,3] Many model compounds have demonstrated oxo-transfer reactions from Me_3NO to desoxo- or monooxomolybdenum(IV) giving monooxo- or dioxomolybdenum(VI) species, respectively.[4−9] Previously, we reported a dioxomolybdenum(VI) benzene-1,2-dithiolate (bdt) complex that oxidized benzoin to benzil with the accompanying production of water, and proceeded in a catalytic cycle similar to a biomimetic enzymatic reaction.[10−12]

NH···S hydrogen bonds are widely distributed in the active sites of enzymes and metalloproteins, as described previously.[13,14] Our systematic investigations revealed the function of the hydrogen bonds using various model compounds of rubredoxins,[13,15] ferredoxins,[16] cytochrome P450s,[17,18] molybdoenzymes,[19,20] and copper proteins.[21] The hydrogen bonds shift the redox potential to more positive values and stabilize M−S bonds.[16,18,22] We found that electron-withdrawing groups enhanced the hydrogen bond, resulting in a greater positive shift of the redox potential, where the change was approximately proportional to the number of hydrogen bonds.[13,16,18]

The introduction of four intramolecular NH···S hydrogen bonds into a monooxomolybdenum(IV) complex, $(NEt_4)_2[Mo^{IV}O(bdt)_2]$, accelerated the reduction of Me_3NO to Me_3N with the accompanying production of the corresponding dioxomolybdenum(VI) complex; however, the results were complicated. The rate constants were dependent on the substituent group R in $(NEt_4)_2[Mo^{IV}O\{S_2\text{-}3,6\text{-}(RCONH)_2C_6H_2\}_2]$, occurring in the order $Ph_3C \gg CH_3 > CF_3 >$ (bdt) > *t*-Bu. This suggested a multiplicity of factors determining the rate constant. Generally, the reduction of Me_3NO by a monooxomolybdenum(IV) complex proceeds via a two-step reaction.[23] First, Me_3NO approaches the molybdenum center from the position *trans* to the oxo ligand, forming a Me_3NO adduct as an intermediate. Next, *trans*−*cis* rearrangement occurs to simultaneously afford a *cis*-dioxo complex and Me_3N. When the concentration of Me_3NO is sufficiently high or the substituent groups are bulky enough (i.e., R = *t*-Bu) to sterically hinder rotation, the *trans*−*cis* rearrangement is the rate-determining step, and saturation of the reaction rate is observed. In the case R = Ph_3C, the situation was very different. The adequately bulky substituent groups prevented rotation and distorted the monooxomolybdenum(IV) complex, which allowed the direct *cis* attack of Me_3NO.[23,24] Unfortunately, the resulting dioxomolybdenum(VI) complexes proved to be too unstable for isolation, and therefore, the contribution of the NH···S in the oxidized state could not be described.

Recently, we successfully isolated a new dioxomolybdenum(VI) complex, which contained two intramolecular NH···S hydrogen bonds, as a single isomer. Through this complex, we revealed the selective and effective stabilization of Mo^{VI}═O by hydrogen bonds.[25] In that report, a carbamoyl group (RNHCO) was used to introduce an amide moiety because of synthetic facility; however, that led to the formation of a flexible NH···S hydrogen bond and resulted in a small contribution to the reduction of Me_3NO in polar solvent.

Received: October 2, 2012
Published: December 21, 2012

dx.doi.org/10.1021/ic302149p | *Inorg. Chem.* 2013, 52, 381−394

In this paper, a series of new ligands with acylamino groups (RCONH; R = CH_3, *t*-Bu, CF_3, CPh_3, $C(C_6H_4$-4-*t*-$Bu)_3$) were designed and synthesized (Figure 1b). The location of the RCONH group at the 3-position of the 1,2-benzenedithiolato ligand provides a rigid and stable intraligand NH···S hydrogen bond. Moreover, the five-membered hydrogen bond is reminiscent of the intraligand interaction in the molybdopterin cofactor (Figure 1a). Alteration of the R group can adequately adjust the strength of the hydrogen bond electrostatically by inductive effects. These newly designed ligands enabled quantitative evaluation of the strength of the hydrogen bonds, and they excluded steric hindrance in the molybdenum complexes, resulting in a systematic investigation of the relationship between the strength of the hydrogen bond and the reactivity of the molybdoenzyme models.

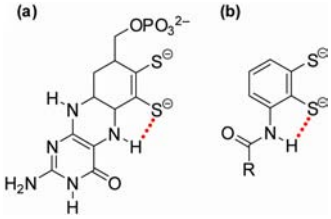

Figure 1. Schematic drawing of (a) molybdopterin and (b) the model ligand having an intramolecular NH···S hydrogen bond.

EXPERIMENTAL SECTION

All procedures were performed under Ar atmosphere by Schlenk technique except extraction.

Materials. Tris(4-*tert*-butylphenyl)methane,[26] 2,3-bis(isopropylthio)benzoic acid,[27] $(NEt_4)[Mo^{V}O(SPh)_4]$,[28] $(NEt_4)_2[Mo^{IV}O(S\text{-}4\text{-}ClC_6H_4)_4]$,[29] and Ph_3CCOCl[13] were prepared by the reported methods.

Synthesis of Tris(4-*tert*-butylphenyl)acetic Acid. Lithiation was carried out in a similar manner as described in the literature.[26] Tris(4-*tert*-butylphenyl)methane (16.5 g, 40.0 mmol) was dissolved in a mixture of dry tetrahydrofuran (THF, 200 mL) and hexamethylphosphoramide (HMPA, 66 mL) and cooled at −70 °C. To this solution was added *n*-butyllithium in *n*-hexane (1.67 M, 26 mL, 43 mmol). The color of the solution turned dark blood red. The solution was stirred at −40 °C for 2 h. Thereafter, dry CO_2 gas was bubbled through the reaction mixture at −30 °C for 30 min, and the solution was warmed up to room temperature to give a yellow solution. The reaction mixture was treated carefully with a piece of ice and conc. HCl aq cooling in an ice bath. The resulting white powder was filtered, washed with THF and *n*-hexane, dried over P_2O_5 in vacuo. Yield: 18.2 g (quant.). Mp: > 300 °C. ^{1}H NMR (DMSO-d_6): δ 13.0 (br, 1H, COOH), 7.31 (d, J = 8.5 Hz, 6H, Ar−H), 7.06 (d, J = 8.5 Hz, 6H, Ar−H), 1.27 (s, 27H, *t*-Bu). FT-IR (KBr): ν(C═O) 1699 cm^{-1}. Anal. Calcd for $C_{32}H_{40}O_2$: C, 84.16; H, 8.83. Found: C, 81.57; H, 9.06.

***N*-{2,3-Bis(isopropylthio)phenyl}carbamoyl Azide (1).** To a solution of 2,3-bis(isopropylthio)benzoic acid (6.19 g, 22.9 mmol) in CH_2Cl_2 (75 mL) was added $SOCl_2$ (60 mL, 830 mmol) and DMF (1.0 mL), and the mixture was refluxed for 3 h. The solution was concentrated to dryness under reduced pressure. The resulting reddish orange residue was dissolved in acetone (100 mL). Cold aqueous solution (25 mL) of NaN_3 (8.99 g, 138 mmol) was added to the solution quickly cooling in an ice bath, and the mixture was stirred at room temperature for 1 h. During the reaction, evolution of nitrogen gas was observed. Cold water (10.0 mL) was added to this solution, and the mixture was stirred for 1.5 h. The solution was stirred at 50 °C for another 30 min and concentrated to dryness under reduced pressure. The residue was dissolved in ethyl acetate. The solution was washed successively with 4% $NaHCO_3$ aq (40 mL × 2), water (30 mL × 2), and sat. NaCl aq (30 mL × 3). The solution was dried over Na_2SO_4 and concentrated to dryness under the reduced pressure. The crude product was purified by column chromatography on silica gel with *n*-hexane/ethyl acetate (49/1) as eluent. The first fraction was collected and concentrated to dryness under reduced pressure to give orange oil. The oil was crystallized from methanol to give colorless crystals. Yield: 2.90 g (41%). ^{1}H NMR ($CDCl_3$): δ 8.60 (br, 1H, NH), 8.06 (d, J = 8.17 Hz, 1H, Ar−H), 7.30 (t J = 8.23 Hz, 1H, Ar−H), 7.00 (dd, J = 8.05, 1.04 Hz, 1H, Ar−H), 3.49 (sep, J = 6.65 Hz, 1H, CH), 3.36 (sep, J = 6.71 Hz, 1H, CH), 1.38 (d, J = 6.65, 6H, CH_3), 1.25 (d, J = 6.71, 6H, CH_3). ESI-MS ([M] = $N_3CONHC_6H_3(SC_3H_7)_2$): m/z 290.1 ($[M\text{-}HN_3+Na^+]^+$, calcd. 290.1), 268.1 ($[M\text{-}HN_3+H^+]^+$, calcd. 268.1). FT-IR (KBr): ν(NH) 3315, ν_{as}(N═N═N) 2142, ν(C═O) 1722 cm^{-1}. Anal. Calcd for $C_{13}H_{18}N_4OS_2$: C, 50.30; H, 5.84; N, 18.05. Found: C, 50.34; H, 5.73; N, 18.04.

2,3-Bis(isopropylthio)aniline (2). This compound was synthesized by a similar procedure to the literature.[30] Compound **1** (602 mg, 1.94 mmol) was dissolved in a mixture of 2.1 M NaOH aq (6.0 mL) and dioxane (6.0 mL). The solution was stirred at room temperature for 45 min. Hydrochloric acid (6 M, 6.0 mL) was added, and the solution was stirred for 30 min. Aqueous NaOH solution (2.1 M, 15.0 mL) was added, and the solution was stirred for 35 min. The mixture was extracted with diethyl ether. The organic layer was washed with water (20 mL × 2) and sat. NaCl aq (15 mL × 3), and then dried over Na_2SO_4. The solution was concentrated to dryness under reduced pressure to give clear oil. The oil was crystallized from diethyl ether to afford colorless crystals. Yield: 425 mg (91%). ^{1}H NMR ($CDCl_3$): δ 7.05 (t, J = 7.93 Hz, 1H, Ar−H), 6.62 (dd, J = 7.93, 0.43 Hz,1H, Ar−H), 6.52 (dd, J = 7.93, 1.22 Hz,1H, Ar−H), 4.51 (br, 2H, Ar-NH_2), 3.43 (sep, J = 6.77 Hz, 1H, CH), 3.41 (sep, J = 6.77 Hz, 1H, CH), 1.38 (d, J = 6.77 Hz,6H, CH_3), 1.26 (d, J = 6.65 Hz,6H, CH_3). Anal. Calcd for $C_{12}H_{19}NS_2$: C, 59.70; H, 7.93; N, 5.80. Found: C, 59.70; H, 7.94; N, 5.79.

***N*-{2,3-Bis(isopropylthio)phenyl}acetamide (3a).** This compound was synthesized by a similar method to the literature.[31] The amine **2** (412 mg, 1.71 mmol) was dissolved in acetic anhydride (10 mL) at room temperature. After stirring at 90 °C for 105 min, unreacted acetic anhydride was hydrolyzed by the addition of water (6 mL) and heating at 60 °C for 30 min. The solution was concentrated to dryness under reduced pressure. The residue was dissolved in diethyl ether (50 mL). The solution was washed with 2% HCl aq (10 mL × 3), 4% $NaHCO_3$ aq (10 mL × 3), water (10 mL × 5), and sat. NaCl aq (10 mL × 2), and then dried over Na_2SO_4. The solution was concentrated to dryness under reduced pressure to give a colorless oily residue. It was crystallized from diethyl ether to give colorless crystals. Yield: 510 mg (quant.). ^{1}H NMR ($CDCl_3$): δ 8.91 (br, 1H, NH), 8.25 (d, J = 8.17 Hz, 1H, Ar−H), 7.28 (t, J = 8.17 Hz, 1H, Ar−H), 6.99 (d, J = 8.17 Hz, 1H, Ar−H), 3.49 (sep, J = 6.85 Hz, 1H, CH), 3.37 (sep, J = 6.85 Hz, 1H, CH), 2.21 (s, 1H, CH_3), 1.38 (d, J = 6.85, 6H, CH_3), 1.26 (d, J = 6.85, 6H, CH_3). FT-IR (CH_2Cl_2): ν(NH) 3338 cm^{-1}. Anal. Calcd for $C_{14}H_{21}NOS_2$: C, 59.32; H, 7.47; N, 4.94. Found: C, 59.32; H, 7.49; N, 4.92.

***N*-{2,3-Bis(isopropylthio)phenyl}pivalamide (3b).** To a THF solution (10 mL) of **2** (142 mg, 0.59 mmol) were added dropwise NEt_3 (0.2 mL, 1.48 mmol) and *t*-BuCOCl (0.18 mL, 1.48 mmol) in an ice bath. The solution was stirred overnight at room temperature and concentrated to dryness under reduced pressure to give an orange powder. The residue was dissolved in ethyl acetate (40 mL). The solution was washed with 2% HCl aq (10 mL × 3), 4% $NaHCO_3$ aq (10 mL × 3), water (10 mL × 3), and sat. NaCl aq (10 mL × 3), and then dried over Na_2SO_4. The solution was concentrated to dryness under reduced pressure to give orange needles. Recrystallization from diethyl ether gave colorless blocks. Yield: 192 mg (quant.). ^{1}H NMR ($CDCl_3$): δ 9.35 (br, 1H, NH), 8.34 (dd, J = 8.00, 1.20 Hz, 1H, Ar−H), 7.28 (t, J = 8.00 Hz, 1H, Ar−H), 6.98 (dd, J = 8.00, 1.20 Hz, 1H, Ar−H), 3.49 (sep, J = 6.65 Hz, 1H, CH), 3.39 (sep, J = 6.65 Hz, 1H, CH), 1.38 (d, J = 6.70 Hz, 6H, CH_3), 1.34 (s, 9H, *t*-Bu), 1.26 (d, J = 6.70 Hz, 6H, CH_3). ESI-MS ([M] = *t*-$BuCONHC_6H_3(SC_3H_7)_2$): m/z 326.2 $(M + H^+)^+$, 348.2 $(M + Na^+)^+$. FT-IR (CH_2Cl_2): ν(NH) 3343

dx.doi.org/10.1021/ic302149p | *Inorg. Chem.* 2013, 52, 381−394

cm^{-1}. Anal. Calcd for $C_{17}H_{27}NS_2$: C, 62.72; H, 8.36; N, 4.30. Found: C, 62.63; H, 8.21; N, 4.33.

***N*-{2,3-Bis(isopropylthio)phenyl}trifluoroacetamide (3c).** This compound was synthesized by a similar method to the literature.[13] To a solution of **2** (435 mg, 1.8 mmol) in THF (15 mL) was added trifluoroacetic anhydride (1.25 mL) at 0 °C. The solution was stirred overnight at 25 °C. Water (8 mL) was added, and the resulting solution was concentrated to dryness under reduced pressure. The residue was dissolved in a mixture of diethyl ether and water. The organic layer was separated and washed with 2% HCl aq (10 mL × 2), 4% $NaHCO_3$ aq (20 mL × 2), water (10 mL × 2), and sat. NaCl aq (10 mL × 2). The solution was dried over Na_2SO_4 and concentrated to dryness under reduced pressure to give brown oil. Yield: 556 mg (92%). ^{1}H NMR ($CDCl_3$): δ 9.93 (br, 1H, NH), 8.22 (dd, J = 8.23, 1.10 Hz, 1H, Ar−H), 7.35 (t, J = 8.23 Hz, 1H, Ar−H), 7.12 (dd, J = 8.23, 1.10 Hz, 1H, Ar−H), 3.51 (sep, J = 6.71 Hz, 1H, CH), 3.39 (sep, J = 6.65 Hz, 1H, CH), 1.38 (d, J = 6.65, 6H, CH_3), 1.26 (d, J = 6.71, 6H, CH_3). ESI-MS ([M] = $CF_3CONHC_6H_3(SC_3H_7)_2$): m/z 338.0 $(M + H^+)^+$, 360.1 $(M + Na^+)^+$. FT-IR (CH_2Cl_2): ν(NH) 3286 cm^{-1}. Anal. Calcd $C_{14}H_{18}F_3NOS_2$: C, 49.83; H, 5.38; N, 4.15. Found: C, 50.17; H, 5.36; N, 4.11.

***N*-{2,3-Bis(isopropylthio)phenyl}-2,2,2-triphenylacetamide (3d).** A solution of Ph_3CCOCl (102 mg, 0.33 mmol) in THF was added dropwise to a solution of **2** (53 mg, 0.22 mmol) and NEt_3 (0.05 mL, 0.4 mmol) in THF (2 mL) at 0 °C. The solution was stirred overnight at 70 °C and concentrated to dryness under reduced pressure. The residue was dissolved in a mixture of diethyl ether and water. The organic layer was separated and washed with 2% HCl aq (20 mL × 2), 4% $NaHCO_3$ aq (20 mL × 2), water (20 mL × 2), and sat. NaCl aq (20 mL × 2). The solution was dried over Na_2SO_4 and concentrated to dryness under reduced pressure to give a colorless powder. The powder was recrystallized from ethyl acetate to give colorless needles. Yield: 59 mg (51%). ^{1}H NMR ($CDCl_3$): δ 9.29 (br, 1H, NH), 8.48 (dd, J = 8.29, 1.16 Hz, 1H, Ar−H), 7.31 (m, 15H, Ar−H(CPh_3)), 7.18 (m, 1H, Ar−H), 6.95 (m, 1H, Ar−H), 3.47 (sep, J = 6.65 Hz, 1H, CH), 3.11 (sep, J = 6.71 Hz, 1H, CH), 1.35 (d, J = 6.65 Hz, 6H, CH_3), 0.85 (d, J = 6.71 Hz, 6H, CH_3). FT-IR (CH_2Cl_2): ν(NH) 3293 cm^{-1}. Anal. Calcd. $C_{32}H_{33}NOS_2$: C, 75.10; H, 6.50; N, 2.74. Found: C, 75.00; H, 6.39; N, 2.82.

***N*-{2,3-Bis(isopropylthio)phenyl}-2,2,2-tris(4-*tert*-butylphenyl)acetamide (3e).** Tris(4-*tert*-butylphenyl)acetic acid (386 mg, 0.85 mmol) was dissolved in $SOCl_2$ (3 mL, 40 mmol), and the solution was stirred at 80 °C for 1.5 h. The solution was concentrated to dryness under reduced pressure to give a white powder, which was dissolved in $CHCl_3$ (5 mL). The solution was added dropwise to a solution of **2** (204 mg, 0.85 mmol) and NEt_3 (0.2 mL, 1 mmol) in $CHCl_3$ (3 mL) at 0 °C. The solution was stirred overnight at 70 °C and concentrated to dryness under reduced pressure. The residue was dissolved in a mixture of *n*-hexane/diethyl ether (1:1) and water. The organic layer was washed successively with 2% HCl aq, 4% $NaHCO_3$ aq, water, and sat. NaCl aq. The solution was dried over Na_2SO_4 and concentrated to dryness under reduced pressure to give a powder. The product was recrystallized from diethyl ether/MeOH to give colorless needles. Yield: 250 mg (48%). ^{1}H NMR ($CDCl_3$): δ 9.32 (br, 1H, NH), 8.50 (dd, J = 8.17, 1.10 Hz, 1H, Ar−H), 7.31, 7.21 (m, 12H, Ar−H ($C(4\text{-}t\text{-}BuC_6H_4)_3$)), 7.27 (t, J = 8.17 Hz, 1H, Ar−H), 6.94 (dd, J = 8.17, 1.10 Hz, 1H, Ar−H), 3.45 (sep, J = 6.65 Hz, 1H, CH), 3.11 (sep, J = 6.65 Hz, 1H, CH), 1.35 (d, J = 6.65 Hz, 6H, CH_3), 1.31 (s, 27H, *t*-Bu), 0.87 (d, J = 6.65 Hz, 6H, CH_3). FT-IR (CH_2Cl_2): ν(NH) 3294 cm^{-1}. Anal. Calcd. $C_{44}H_{57}NOS_2$: C, 77.71; H, 8.45; N, 2.06. Found: C, 76.13; H, 8.28; N, 1.17.

$(1,2\text{-}S_2\text{-}3\text{-}CH_3CONHC_6H_3)_2$ (4a). A solution of **3a** (177 mg, 0.62 mmol) in THF (1.5 mL) was added dropwise to a solution of sodium (152 mg, 6.61 mmol) in liquid NH_3 (about 50 mL). After stirring for 30 min, the reaction was quenched with NH_4Cl (180 mg, 3.37 mmol). Upon quenching, the color turned from blue to colorless. The solvent was removed, and the residue was redissolved in water (60 mL). The solution was washed with diethyl ether (30 mL) and stirred in air at room temperature (r.t.) for 4 days. The precipitated yellow powder was collected by centrifugation and washed with water. The product was dried over P_2O_5 under reduced pressure. Yield: 103.6 mg (85%). ^{1}H NMR ($CDCl_3$): δ 8.74, 8.71 (br, 1H, NH (*cis*, *trans*)), 8.62, 8.58 (d, J = 8.48, Hz, 1H, Ar−H (*cis*, *trans*)), 7.55, 7.50 (dd, J = 7.56, 1.46 Hz, 1H, Ar−H (*cis*, *trans*)), 7.37, 7.36 (t, J = 8.05 Hz, 1H, Ar−H (*cis*, *trans*)), 2.32, 2.29 (s, 3H, CH_3 (*cis*, *trans*)). ESI-MS ([M] = $(1,2\text{-}S_2\text{-}3\text{-}CH_3CONHC_6H_3)_2$): m/z 417.2 $(M + Na^+)^+$.

$(1,2\text{-}S_2\text{-}3\text{-}t\text{-}BuCONHC_6H_3)_2$ (4b). A solution of **3b** (183 mg, 0.56 mmol) in THF (2.0 mL) was added dropwise to a solution of sodium (54 mg, 2.30 mmol) in liquid NH_3 (~50 mL). After stirring for 20 min, the reaction was quenched with NH_4Cl (69 mg, 1.30 mmol). The solvent was removed, and the residue was dissolved in water (30 mL). The solution was washed with diethyl ether (20 mL) and stirred in the air at r.t. for 2 days. The precipitation was collected by centrifugation and washed with water and sat. NaCl aq. The product was dried over P_2O_5 under reduced pressure to give a pale yellow powder. Yield: 63 mg (47%). ^{1}H NMR ($CDCl_3$): δ 9.20, 9.14 (br, 1H, NH (*cis*, *trans*)), 8.65, 8.59 (dd, J = 8.40, 1.40 Hz, 1H, Ar−H (*cis*, *trans*)), 7.54, 7.48 (dd, J = 8.40, 1.40 Hz, 1H, Ar−H (*cis*, *trans*)), 7.38, 7.36 (t, J = 8.40 Hz, 1H, Ar−H (*cis*, *trans*)), 1.39 (s, 9H, *t*-Bu). ESI-MS ([M] = $(1,2\text{-}S_2\text{-}3\text{-}t\text{-}BuCONHC_6H_3)_2$): m/z 479.2 $(M + H^+)^+$, 496.1 $(M + NH_4^+)^+$, 501.3 $(M + Na^+)^+$.

$(1,2\text{-}S_2\text{-}3\text{-}NH_2C_6H_3)_2$. The compound **4a** (205.5 mg, 0.52 mmol) was dissolved in conc. HCl aq (~5 mL), and the solution was stirred at 50 °C for 2 days. The solution was basified by NaOH aq in an ice bath to give yellow powder. The precipitate was collected by centrifugation and washed with water. The yellow powder was dried over P_2O_5 under reduced pressure. Yield: 227.5 mg (quant). ^{1}H NMR ($CDCl_3$): δ 7.15 (dd, J = 7.44, 1.46 Hz, 1H, Ar−H), 7.08 (t, J = 8.05, 7.44 Hz, 1H, Ar−H), 6.77 (dd, J = 8.05, 1.46 Hz, 1H, Ar−H), 4.72 (br, 2H, NH_2). ESI-MS([M] = $(1,2\text{-}S_2\text{-}3\text{-}NH_2C_6H_3)_2$) m/z 309.4 $(M - H^+)^-$.

$(1,2\text{-}S_2\text{-}3\text{-}CF_3CONHC_6H_3)_2$ (4c). Trifluoroacetic anhydride (1 mL) was added to a solution of $(1,2\text{-}S_2\text{-}3\text{-}NH_2C_6H_3)_2$ (102.7 mg, 0.33 mmol) in THF (25 mL) cooling in an ice bath. The reaction mixture was stirred at 30 °C overnight. The unreacted $(CF_3CO)_2O$ was hydrolyzed by the addition of water. The solution was concentrated to dryness under reduced pressure to give an off-white powder. The powder was dissolved in diethyl ether and washed with 2% HCl aq, 4% $NaHCO_3$ aq, water, and sat. NaCl aq. The organic layer was dried over Na_2SO_4. The solution was concentrated to dryness under reduced pressure to give an off-white powder, which was dried over P_2O_5 under reduced pressure. Yield: 44 mg (27%). ^{1}H NMR ($CDCl_3$): δ 9.58, 9.48 (br, 1H, NH (*cis*, *trans*)), 8.59, 8.56 (dd, J = 8.36, 1.34 Hz, 1H, Ar−H (*cis*, *trans*)), 7.70, 7.68 (dd, J = 8.36, 1.34 Hz, 1H, Ar−H (*cis*, *trans*)), 7.49, 7.48 (t, J = 8.36 Hz, 1H, Ar−H (*cis*, *trans*)). ESI-MS ([M] = $(1,2\text{-}S_2\text{-}3\text{-}CF_3CONHC_6H_3)_2$): m/z 501.4 $(M - H^+)^-$.

$(1,2\text{-}S_2\text{-}3\text{-}Ph_3CCONHC_6H_3)_2$ (4d). A solution of Ph_3CCOCl (370 mg, 1.21 mmol) in THF (5 mL) was added dropwise to a solution of $(1,2\text{-}S_2\text{-}3\text{-}NH_2C_6H_3)_2$ (185 mg, 0.60 mmol) and NEt_3 (0.2 mL, 1.4 mmol) in THF (5 mL) in an ice bath, and the reaction mixture was stirred at 70 °C for 4 days. A yellow precipitate was deposited gradually, which was collected with filtration and washed with THF to give a yellow powder. The powder was dried over P_2O_5 under reduced pressure. Yield: 210 mg (41%). ^{1}H NMR ($CDCl_3$): δ 9.13 (br, 1H, NH), 8.72 (dd, J = 8.11, 1.71 Hz, 1H, Ar−H), 7.35 (m, 17H, Ar−H + Ar−H(CPh_3)). ESI-MS ([M] = $(1,2\text{-}S_2\text{-}3\text{-}Ph_3CCONHC_6H_3)_2$): m/z 849.4 $(M - H^+)^-$.

$\{1,2\text{-}S_2\text{-}3\text{-}(4\text{-}t\text{-}Bu\text{-}C_6H_4)_3CCONHC_6H_3\}_2$ (4e). A solution of $(4\text{-}t\text{-}Bu\text{-}C_6H_4)_3CCOCl$ (570 mg, 1.20 mmol) in CH_2Cl_2 (5 mL) was added dropwise to a solution of $(1,2\text{-}S_2\text{-}3\text{-}NH_2C_6H_3)_2$ (187 mg, 0.60 mmol) and NEt_3 (0.2 mL, 1.4 mmol) in CH_2Cl_2 (5 mL) cooling in an ice bath, and the reaction mixture was stirred at 50 °C for 4 days. A yellow precipitate was deposited gradually, which was collected by filtration, and washed with ethyl acetate to give a yellow powder. The powder was dried over P_2O_5 under reduced pressure. Yield: 140 mg (25%). ^{1}H NMR ($CDCl_3$): δ 9.29 (br, 1H, NH), 8.78 (d, J = 5.67 Hz, 1H, Ar−H), 7.36−7.24 (m, 14H, Ar−H + Ar−H ($C(4\text{-}t\text{-}BuC_6H_4)_3$), 1.33 (s, 27H, *t*-Bu). ESI-MS ([M] = $\{1,2\text{-}S_2\text{-}3\text{-}(4\text{-}t\text{-}Bu\text{-}C_6H_4)_3CCONHC_6H_3\}_2$) m/z = 1209.6 $(M + Na)^+$.

dx.doi.org/10.1021/ic302149p | *Inorg. Chem.* 2013, 52, 381−394

$(NEt_4)_2[Mo^{IV}O(1,2\text{-}S_2\text{-}3\text{-}CH_3CONHC_6H_3)_2]$ (5a). A mixture of $(NEt_4)_2[Mo^{IV}O(S\text{-}4\text{-}ClC_6H_4)_4]$ (36 mg, 0.038 mmol) and **4a** (15 mg, 0.038 mmol) in MeCN (3 mL) was stirred at room temperature overnight. The insoluble materials were filtered out. The filtrate was concentrated to a volume of 1 mL, and diethyl ether was added to the solution to give an orange powder. The powder was collected, and washed with 1,2-dimethoxyethane (DME), then dissolved in acetonitrile. The solution was filtered, and the filtrate was concentrated under reduced pressure to a minimum volume. Upon cooling in the refrigerator, an orange powder was deposited. This powder was separated and dried in vacuo. Yield: 10 mg (33%). ^{1}H NMR (CD_3CN): δ 8.93 (br, 1H, NH), 7.72 (d, J = 7.7 Hz, 1H, Ar−H), 7.23 (d, J = 7.7 Hz, 1H, Ar−H), 6.71 (t, J = 7.7 Hz, 1H, Ar−H), 2.97 (q, J = 7.2 Hz, 8H, NEt_4), 2.13 (s, 3H, CH_3), 1.03 (tt, J = 7.2, 1.8 Hz, 12H, NEt_4). ESI-MS (M^{2-} = $[Mo^{IV}O(1,2\text{-}S_2\text{-}3\text{-}CH_3CONHC_6H_3)_2]^{2-}$): m/z 509.3 $(M^{2-} + H^+)^-$, 638.0 $(M^{2-} + (NEt_4)^+)^-$. Absorption spectrum (DMF): λ_{max} (ε, M^{-1} cm^{-1}) 331 (8400), 382 (sh) (850), 448 (370) nm. Anal. Calcd for $C_{32}H_{54}MoN_4O_3S_4$: C, 50.11; H, 7.10; N, 7.30. Found: C, 48.48; H, 6.68; N, 6.89.

The disagreement of elemental analysis for molybdenum complexes is probably caused by their air sensitivity and low crystallinity. Unfortunately, trials for crystallization of the complexes failed. The powder was oxidized easily and increase in weight was observed during weighing. Formal addition of oxygen to the chemical formula improved the results. The calculated values for $C_{32}H_{54}MoN_4O_3S_4{\cdot}(O_2)_{0.8}$: C, 48.49; H, 6.87; N, 7.07, which agree with the found ones.

$(NEt_4)_2[Mo^{IV}O(1,2\text{-}S_2\text{-}3\text{-}t\text{-}BuCONHC_6H_3)_2]$ (5b). This compound was synthesized by a similar method to the literature.[24] To a solution of $(NEt_4)[Mo^{V}O(SPh)_4]$ (100 mg, 0.15 mmol) in acetonitrile (3 mL) were added a solution of **4b** (70 mg, 0.15 mmol) and tetraethylammonium borohydride (22 mg, 0.15 mmol) in acetonitrile (3 mL) and water (0.6 mL). The solution was stirred overnight, and then the solution was concentrated to dryness under reduced pressure. The residue was washed with DME, and dissolved in acetonitrile. After removal of insoluble materials with filtration, the filtrate was concentrated under reduced pressure and then refrigerated to give orange powder. This powder was dried in vacuo. Yield: 52 mg (49%). ^{1}H NMR (CD_3CN): δ 9.40, 9.38 (br, 1H, NH (*cis*, *trans*)), 7.89, 7.88 (dd, J = 7.6, 1.2 Hz, 1H, Ar−H (*cis*, *trans*)), 7.32, 7.31 (dd, J = 7.6, 1.2 Hz, 1H, Ar−H (*cis*, *trans*)), 6.80, 6.79 (t, J = 7.6 Hz, 1H, Ar−H (*cis*, *trans*)), 2.99 (q, J = 7.2 Hz, 8H, CH_2 (NEt_4)), 1.40, 1.39 (s, 9H, *t*-Bu (*cis*, *trans*)), 1.08 (tt, J = 7.2, 1.7 Hz, 12H, CH_3 (NEt_4)). ESI-MS (M^{2-} = $[Mo^{IV}O(1,2\text{-}S_2\text{-}3\text{-}t\text{-}BuCONHC_6H_3)_2]^{2-}$) m/z 296.3 (M^{2-}), 592.5 $(M^{2-} + H^+)^-$, 722.3 $(M^{2-} + (NEt_4)^+)^-$. Absorption spectrum (DMF): λ_{max} (ε, M^{-1} cm^{-1}) 331 (8800), 382 (sh) (930), 448 (440) nm. Anal. Calcd for $C_{38}H_{66}MoN_4O_3S_4$: C, 53.62; H, 7.82; N, 6.58. Found: C, 49.78; H, 7.56; N, 5.94.

The following method also gave the identical product, which was confirmed by spectral measurements. A mixture of $(NEt_4)_2[Mo^{IV}O(S\text{-}4\text{-}ClC_6H_4)_4]$ (39 mg, 0.041 mmol) and **4b** (20 mg, 0.041 mmol) in DME (3 mL) was stirred at room temperature overnight. The precipitated orange powder was collected and washed with DME. The crude product was purified by reprecipitation from acetonitrile/diethyl ether to give pure **5b**. Yield: 11 mg (32%).

$(NEt_4)_2[Mo^{IV}O(1,2\text{-}S_2\text{-}3\text{-}CF_3CONHC_6H_3)_2]$ (5c). A mixture of $(NEt_4)_2[Mo^{IV}O(S\text{-}4\text{-}ClC_6H_4)_4]$ (126 mg, 0.13 mmol) and **4c** (67 mg, 0.13 mmol) in DME (5 mL) was stirred at room temperature for 3 h. Orange powder was precipitated from the reaction mixture, which was collected and washed with DME. The powder was purified by a similar procedure described for **5a**. The resulting orange powder was dried in vacuo. Yield: 29 mg (27%). ^{1}H NMR (CD_3CN): δ 10.02 (br, 1H, NH (*cis*, *trans*)), 7.75 (dd, J = 7.7, 1.2 Hz, 1H, Ar−H (*cis*, *trans*)), 7.47, 7.46 (dd, J = 7.7, 1.2 Hz, 1H, Ar−H (*cis*, *trans*)), 6.88 (t, J = 7.7 Hz, 1H, Ar−H (*cis*, *trans*)), 3.07 (q, J = 7.3 Hz, 8H, $CH_2(NEt_4)$), 1.14 (tt, J = 7.3, 1.9 Hz, 12H, $CH_3(NEt_4)$). ESI-MS (M^{2-} = $[Mo^{IV}O(1,2\text{-}S_2\text{-}3\text{-}CF_3CONHC_6H_3)_2]^{2-}$) m/z 616.3 $(M^{2-} + H^+)^-$, 746.0 $(M^{2-} + (NEt_4)^+)^-$. Absorption spectrum (DMF): λ_{max} (ε, M^{-1} cm^{-1}) 286 (26600), 342 (5800), 435 (670) nm. Anal. Calcd for $C_{32}H_{48}F_6MoN_4O_3S_4$: C, 43.93; H, 5.53; N, 6.40. Found: C, 43.46; H, 5.34; N, 6.36.

$(NEt_4)_2[Mo^{IV}O(1,2\text{-}S_2\text{-}3\text{-}Ph_3CCONHC_6H_3)_2]$ (5d). A mixture of $(NEt_4)_2[Mo^{IV}O(S\text{-}4\text{-}ClC_6H_4)_4]$ (93 mg, 0.10 mmol) and **4d** (83 mg, 0.10 mmol) in DME (5 mL) was stirred at room temperature overnight. Grayish orange powder was deposited from the reaction mixture, which was collected and washed successively with DME, acetonitrile, toluene, and acetonitrile. The orange powder was dried in vacuo. Yield: 27.3 mg (23%). ^{1}H NMR (CD_3CN): δ 9.32 (br, 1H, NH), 7.90, 7.87 (dd, J = 7.7, 1.2 Hz, 1H, Ar−H (*cis*, *trans*)), 7.50−7.25 (m, 16H, Ar−H + CPh_3(*cis*, *trans*)), 6.78, 6.77 (t, J = 7.7 Hz,, 1H, Ar−H (*cis*, *trans*)), 2.97 (q, J = 7.3 Hz, 8H, $CH_2(NEt_4)$), 1.06 (tt, J = 7.3, 1.8 Hz, 12H, $CH_3(NEt_4)$). ESI-MS (M^{2-} = $[Mo^{IV}O(1,2\text{-}S_2\text{-}3\text{-}CPh_3CONHC_6H_3)_2]^{2-}$) m/z 964.4 $(M^{2-} + H^+)^-$, 1094.3 $(M^{2-} + (NEt_4)^+)^-$. Absorption spectrum (DMF): λ_{max} (ε, M^{-1} cm^{-1}) 342 (8300), 402 (700), 448 (sh) (450) nm. Anal. Calcd for $C_{68}H_{78}MoN_4O_3S_4$: C, 66.75; H, 6.43; N, 4.58. Found: C, 64.80; H, 6.09; N, 4.66.

$(NEt_4)_2[Mo^{IV}O\{1,2\text{-}S_2\text{-}3\text{-}(4\text{-}t\text{-}BuC_6H_4)_3CCONHC_6H_3\}_2]$ (5e). A mixture of $(NEt_4)_2[Mo^{IV}O(S\text{-}4\text{-}ClC_6H_4)_4]$ (211 mg, 0.22 mmol) and **4e** (267 mg, 0.25 mmol) in DME (8 mL) was stirred at room temperature for 2 h. The grayish red powder was precipitated from the reaction mixture, which was collected and washed with DME and propionitrile. The obtained orangish white powder was dried in vacuo. Yield: 91 mg (26%). ^{1}H NMR (CD_3CN): δ 9.43 (br, 1H, NH), 7.90 (dd, J = 7.6, 1.1 Hz, 1H, Ar−H), 7.39 (dd, J = 39.1, 21.7 Hz,12H, Ar−H((4-*t*-$BuC_6H_4)_3C$)), 7.26 (dd, J = 7.6, 1.1 Hz, 1H, Ar−H), 6.76 (t, J = 7.6 Hz, 1H, Ar−H), 3.10 (q, J = 7.3 Hz, 8H, $CH_2(NEt_4)$), 1.35 (s, 27H, *t*-Bu), 1.16 (tt, J = 7.3, 1.9 Hz, 12H, $CH_3(NEt_4)$). ESI-MS (M^{2-} = $[Mo^{IV}O(1,2\text{-}S_2\text{-}3\text{-}(4\text{-}t\text{-}BuC_6H_4)_3CCONHC_6H_3)_2]^{2-}$) m/z 1300.9 $(M^{2-} + H^+)^-$, 1430.8 $(M^{2-} + (NEt_4)^+)^-$. Absorption spectrum (DMF): λ_{max} (ε, M^{-1} cm^{-1}) 289 (33100), 343 (8100), 400 (sh) (780), 446 (sh) (440) nm.

$(NEt_4)_2[Mo^{VI}O_2(1,2\text{-}S_2\text{-}3\text{-}CH_3CONHC_6H_3)_2]$ (6a). To a DMF solution (2 mL) of **5a** (2.9 mg, 0.0038 mmol) was added a DMF solution (0.2 mL) containing 0.57 mg (0.0076 mmol) of trimethylamine *N*-oxide at room temperature. The pale yellow solution turned immediately to red. The solution was concentrated to dryness under reduced pressure. The residue was washed with DME and dried under reduced pressure. The product was used for the spectral measurements without further purification. ^{1}H NMR (CD_3CN): δ 8.43 (br, 1H, NH), 7.70 (d, J = 7.8 Hz, 1H, Ar−H), 6.87 (dd, J = 7.8, 1.3 Hz, 1H, Ar−H), 6.60 (t, J = 7.8 Hz, 1H, Ar−H), 3.12 (q, J = 7.3 Hz, 8H, NEt_4), 2.03 (s, 3H, CH_3), 1.18 (tt, J = 7.3, 1.9 Hz, 12H, NEt_4). ESI-MS (M^{2-} = $[Mo^{VI}O_2(1,2\text{-}S_2\text{-}3\text{-}CH_3CONHC_6H_3)_2]^{2-}$): m/z 654.1 $(M^{2-} + (NEt_4)^+)^-$. Absorption spectrum (DMF): λ_{max} (ε, M^{-1} cm^{-1}) 303 (sh) (14000), 338 (10500), 378 (sh) (5700), 524 (2300) nm.

The following dioxomolybdenum(VI) complexes were synthesized by a similar method described for **6a**.

$(NEt_4)_2[Mo^{VI}O_2(1,2\text{-}S_2\text{-}3\text{-}t\text{-}BuCONHC_6H_3)_2]$ (6b). ^{1}H NMR (CD_3CN): δ 8.82 (br, 1H, NH), 7.81 (dd, J = 7.8, 1.3 Hz, 1H, Ar−H), 6.86 (dd, J = 7.8, 1.3 Hz, 1H, Ar−H), 6.61 (t, J = 7.8 Hz, 1H, Ar−H), 3.11 (q, J = 7.3 Hz, 8H, NEt_4), 1.23 (s, 9H, *t*-Bu), 1.17 (tt, J = 7.3, 1.9 Hz, 12H, NEt_4). ESI-MS (M^{2-} = $[Mo^{VI}O_2(1,2\text{-}S_2\text{-}3\text{-}t\text{-}BuCONHC_6H_3)_2]^{2-}$): m/z 738.3 $(M^{2-} + (NEt_4)^+)^-$. Absorption spectrum (DMF): λ_{max} (ε, M^{-1} cm^{-1}) 303 (sh) (14600), 338 (11700), 377 (sh) (6400), 522 (230) nm.

$(NEt_4)_2[Mo^{VI}O_2(1,2\text{-}S_2\text{-}3\text{-}CF_3CONHC_6H_3)_2]$ (6c). ^{1}H NMR (CD_3CN): δ 9.54 (br, 1H, NH), 7.68 (dd, J = 7.8, 1.3 Hz, 1H, Ar−H), 6.69 (dd, J = 7.8, 1.3 Hz, 1H, Ar−H), 6.61 (t, J = 7.8 Hz, 1H, Ar−H), 3.14 (q, J = 7.3 Hz, 8H, NEt_4), 1.19 (tt, J = 7.3, 1.9 Hz, 12H, NEt_4). Absorption spectrum (DMF): λ_{max} (ε, M^{-1} cm^{-1}) 284 (sh) (20700), 349 (6200), 510 (860) nm.

$(NEt_4)_2[Mo^{VI}O_2(1,2\text{-}S_2\text{-}3\text{-}Ph_3CCONHC_6H_3)_2]$ (6d). ^{1}H NMR (CD_3CN): δ 8.76 (br, 1H, NH), 7.80 (dd, J = 7.8, 1.3 Hz, 1H, Ar−H), 7.31−7.16 (m, 15H, CPh_3), 6.86 (dd, J = 7.8, 1.3 Hz, 1H, Ar−H), 6.62 (t, J = 7.8 Hz, 1H, Ar−H), 2.96 (q, J = 7.3 Hz, 8H, $CH_2(NEt_4)$), 1.06 (tt, J = 7.3, 1.9 Hz, 12H, $CH_3(NEt_4)$). ESI-MS (M^{2-} = $[Mo^{VI}O_2(1,2\text{-}S_2\text{-}3\text{-}Ph_3CCONHC_6H_3)_2]^{2-}$) m/z 981.3 $(M^{2-} + H^+)^-$.

dx.doi.org/10.1021/ic302149p | *Inorg. Chem.* 2013, 52, 381−394

Absorption spectrum (DMF): λ_{max} (ε, M^{-1} cm^{-1}) 283 (sh) (22800), 357 (9400), 410 (sh) (4600), 525 (2100) nm.

$(NEt_4)_2[Mo^{VI}O_2\{1,2\text{-}S_2\text{-}3\text{-}(4\text{-}t\text{-}BuC_6H_4)_3CCONHC_6H_3\}_2]$ (6e). ^1H NMR (CD_3CN): δ 8.82 (br, 1H, NH), 7.76 (dd, J = 7.8, 1.3 Hz, 1H, Ar−H), 7.26 (dd, J = 47.2, 29.5 Hz,12H, Ar−H((4-t-$BuC_6H_4)_3C$)), 6.79 (dd, J = 7.8, 1.3 Hz, 1H, Ar−H), 6.53 (t, J = 7.8 Hz, 1H, Ar−H), 3.11 (q, J = 7.3 Hz, 8H, $CH_2(NEt_4)$), 1.26 (s, 27H, t-Bu), 1.16 (tt, J = 7.3, 1.9 Hz, 12H, $CH_3(NEt_4)$). ESI-MS (M^{2-} = $[Mo^{VI}O_2(1,2\text{-}S_2\text{-}3\text{-}(4\text{-}t\text{-}BuC_6H_4)_3CCONHC_6H_3)_2]^{2-}$) m/z 1576.4 (M^{2-} + 2$(NEt_4)^+$ + $H^+)^+$, 1706.5 (M^{2-} + 3$(NEt_4)^+)^+$. Absorption spectrum (DMF): λ_{max} (ε, M^{-1} cm^{-1}) 356 (8900), 410 (sh) (3400), 528 (1500) nm.

Physical Measurements. ^1H NMR spectra were obtained on a JEOL GSX-400 spectrometer and a JEOL ECA-500 in $CDCl_3$ or CD_3CN at 30 °C. GOESY spectra were recorded on a VARIAN VNS-600. ESI-MS spectrometric analyses were performed on a Finnigan MAT LCQ-MS instrument using acetonitrile solution. IR spectroscopic measurements in solution were done on Jasco FT/IR-4000 spectrometer. Raman spectra were measured at 298 K on Jasco NR-1800 with Liq. N_2 cooled CCD detector. Exciting radiation was provided by Ar^+ ion laser (514.5 nm). The measurement of cyclic voltammograms (CVs) in DMF solution were carried out on a BAS 100B/W instrument with a three-electrode system: glassy carbon working electrode, a Pt-wire auxiliary electrode, and saturated calomel electrode (SCE). The scan rate was 100 mV/s. Concentration of the sample was 2.5 mM, containing 0.1 M of n-Bu_4NClO_4 as a supporting electrolyte. Potential was determined at room temperature vs SCE as a reference. The result was cross-referenced by using the ferrocene/ferrocenium couple as a calibrant. The redox potential of $Fe(Cp)_2$ was observed at +0.48 V vs SCE under the same condition. UV−visible absorption spectra were recorded using a SHIMADZU UV-3100PC spectrometer.

Structural Determination. Each single crystal of **1**, **3a**, **3b**, and **3d** was selected carefully and mounted on MicroMount 200 μm with Nujol, which was frozen immediately in a stream of cold nitrogen at 200 K. Data collection was made on a Rigaku RAPID II Imaging Plate area detector with Mo−Kα radiation (0.71075 Å) using MicroMax-007HF microfocus rotating anode X-ray generator and VariMax-Mo optics. The structure was solved by SIR-92[32] and expanded Fourier technique using SHELXL-97.[33] All non-hydrogen atoms were refined anisotropically. All hydrogen atoms except amide NH of **1**, **3b**, and **3d** were located at the calculated positions using the riding model.

Kinetic Analysis. Reaction systems containing the monooxomolybdenum(IV) complex and Me_3NO were monitored spectrophotometrically in the region 250−700 nm. A typical measurement was carried out using a 1-mm UV cell containing a solution (0.3 mL) of monooxomolybdenum(IV) complex (1 mM in DMF; 0.3 mL) at 27 °C. After thermal equilibrium, a Me_3NO solution (60 mM, 180 mM, 240 mM, 300 mM; 10 μL) was injected through a silicone rubber cap, and the cell contents were quickly mixed by shaking. All calculations for the data analysis were performed at 525 nm for **5a**, 524 nm for **5b**, 525 nm for **5c**, 521.5 nm for **5d**, and 527.5 nm for **5e**.

Density Functional Theory (DFT) Calculations. Geometry optimizations, frequency calculations, and natural bond orbital (NBO) analysis were performed using Becke's three parameter hybrid fuctionals (B3LYP) in the Gaussian 03[34] program package. The basis set used for Mo was MINI-1[35] supplemented by the 5p AO with the same exponent as that for the 5s AO.[36] For the other atoms (H, C, N, O, F, S), a 6-31G** basis set was employed. The coordinates of the crystal structures, $(NEt_4)_2[Mo^{IV}O\{1,2\text{-}S_2\text{-}3,6\text{-}(CH_3CONH)_2C_6H_2\}_2]$,[24] and $(NEt_4)_2[W^{VI}O\{1,2\text{-}S_2\text{-}3,6\text{-}(CH_3CONH)_2C_6H_2\}_2]$[37] were used for the initial structures with some modifications. The intermediates of the reaction between the molybdenum complexes with Me_3NO were calculated using the following procedure. At first, the optimized structures of $[MoO(bdt)_2]^{2-}$ (bdt = 1,2-benzenedithiolato), *trans*-$[Mo^{IV}O(1,2\text{-}S_2\text{-}3\text{-}t\text{-}BuCONHC_6H_3)_2]^{2-}$ (*trans*-**5b**), *cis*-$[Mo^{IV}O(1,2\text{-}S_2\text{-}3\text{-}t\text{-}BuCONHC_6H_3)_2]^{2-}$ (*cis*-**5b**), $[Mo^{IV}O\{1,2\text{-}S_2\text{-}3,6\text{-}(t\text{-}BuCONH)_2C_6H_2\}_2]^{2-}$ (**7b**), and $[Mo^{IV}O(1,2\text{-}S_2\text{-}3\text{-}CF_3CONHC_6H_3)_2]^{2-}$ (**5c**) were obtained. The obtained structures were connected with $ONMe_3$ on the software ChemBio3D Ultra (ver. 11.0), and the energy was minimized by MM2 calculation to give initial models for DFT calculations. The geometry was roughly optimized using a 3-21G basis set and then reoptimized by the higher level basis sets described above.

RESULTS

Synthesis of the Ligands. A series of 3-acylaminobenzenedithiolato ligands was synthesized in a stepwise fashion, as shown in Scheme 1. The well-known Curtius rearrangement,

Scheme 1. Synthetic Route of the Disulfides and the Molybdenum Complexes[a]

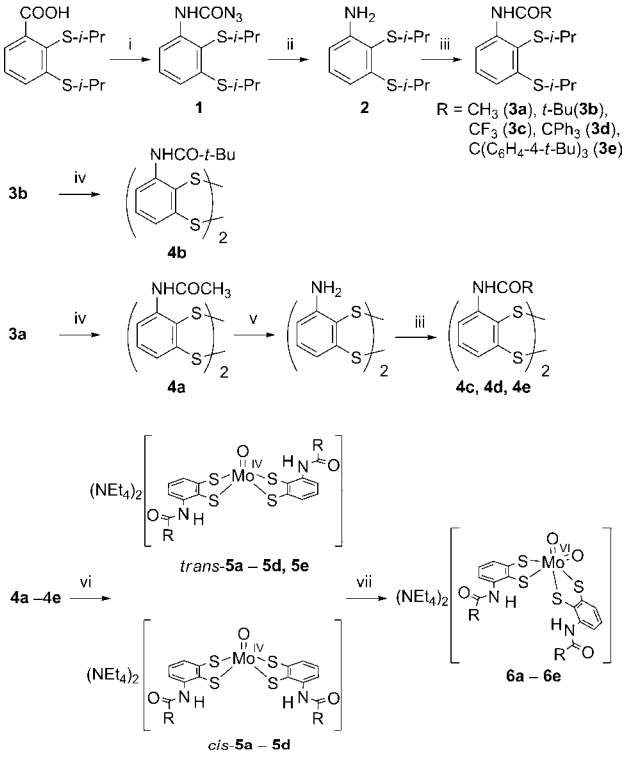

[a](i) $SOCl_2/CH_2Cl_2$, then NaN_3 aq/acetone. (ii) dil. NaOH aq/dioxane, HCl aq, then NaOH aq. (iii) RCOCl or $(RCO)_2O$. (iv) Na/liq. NH_3, then air oxidation. (v) conc. HCl aq, then NaOH aq. (vi) $(NEt_4)_2[MoO(S\text{-}4\text{-}ClC_6H_4)_4]$ in DME (or CH_3CN), or NEt_4BH_4, then $(NEt_4)[MoO(SPh)_4]$ in CH_3CN/H_2O. (vi) Me_3NO/DMF.

which effectively converts a carboxylic acid to an amine, was used to introduce an amino group to the benzene ring.[38−40] In the general procedure, a carboxylic acid is converted to an acid chloride, which is allowed to react with NaN_3 to give a carbazide ($RCON_3$).[38] The carbazide is rearranged to the amine with the evolution of nitrogen gas by heating under acidic conditions. In our case, the carbazide could not be isolated and was converted to the carbamoyl azide in the presence of excess NaN_3 without heating. Carbamoyl azides are known, and their properties have been reviewed.[41] Some derivatives have been structurally characterized by X-ray analysis.[42,43] The isolated *N*-{2,3-bis(isopropylthio)phenyl}-carbamoyl azide (**1**) was fully characterized by ^1H NMR, IR spectroscopy, elemental analysis, and X-ray analysis.

The molecular structure of **1** is shown in Figure 2, and the crystallographic parameters are listed in Supporting Information, Table S1. The geometrical parameters were typical, and no significant differences could be found from the reported structures.[42,43] It was noteworthy that the NH group was

dx.doi.org/10.1021/ic302149p | Inorg. Chem. 2013, 52, 381−394

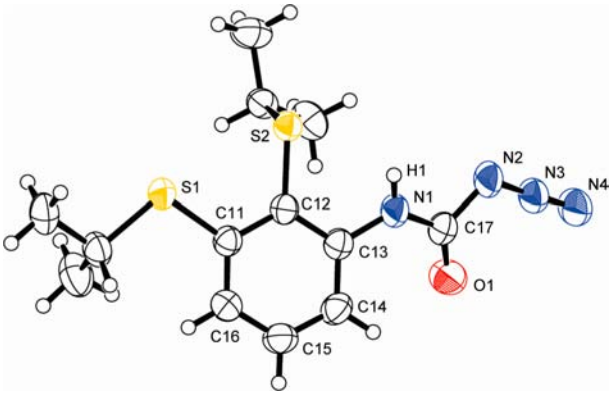

Figure 2. Molecular structure of *N*-[2,3-bis(isopropylthio)phenyl]-carbamoyl azide (**1**).

directed toward the sulfur atom with a H···S distance of 2.53(2) Å, suggesting the presence of a weak NH···S hydrogen bond. The NH group exhibited a ^{1}H NMR signal at 8.60 ppm and ν(NH) at 3315 cm^{-1} in the IR spectrum. The relatively downfield-shifted ^{1}H signal and lower wavenumber ν(NH) characterize the acidic NH group forming the NH···S hydrogen bond.

The Curtius rearrangement generally proceeds at high temperatures or requires protic or Lewis acids as catalysts.[44] In our case, the rearrangement occurred under mild conditions, although the reaction mixture was heated to complete the reaction for practicality. The synthesis of carbamoyl azides from acid chlorides and aqueous NaN_3 at room temperature has been reported.[45] Another paper reported the isolation of carbazide derivatives under mild conditions; however, the IR spectra exhibited a peak at 3294 cm^{-1} which suggests the formation of a carbamoyl azide, which was not mentioned in the paper.[46] These reported compounds contained O or S atoms close to the N atom adjacent to the carbonyl C of the carbazide as a common structure. We present here a proposed mechanism (shown in Supporting Information, Scheme S1). Electron-rich sulfur probably stabilizes the electron-deficient nitrene intermediate concomitant with the evolution of nitrogen gas. The polarized intermediate is readily converted to an isocyanate by 1,2-rearrangemement, which then easily reacts with excess azide anion to give product **1**.

The carbamoyl azide **1** was smoothly hydrolyzed by dilute alkaline solution following the evolution of CO_2 gas under acidic conditions to give the amine **2** in high yield. Acylation of **2** by the corresponding acid chloride or acid anhydride gave **3a**−**3e** in satisfactory yields. These compounds were characterized by ^{1}H NMR, IR spectroscopy, and elemental analysis. For **3a**, **3b**, and **3d**, molecular structures were determined by X-ray analysis. The molecular structures are shown in Supporting Information, Figure S1, and the crystallographic parameters are listed in Supporting Information, Table S1. These structures were essentially the same except that the amide plane of **3a** was twisted (by approximately −50°) from the benzene ring, whereas the amide planes of **3b** and **3d** were nearly coplanar with the benzene ring. The amide NH group of **3a** was directed to the neighboring carbonyl group to form an intermolecular NH···O═C hydrogen bond. The coplanarity of **3b** and **3d** suggested the presence of intramolecular NH···S hydrogen bonds. The S2−C12 distances (1.769−1.779 Å) were longer than the S1−C11 distances (1.764−1.770 Å), and the C12−S2−C4 angles (99.70−103.35°) were smaller than the C11−S1−C1 angles (104.91−105.22°). The longer S2−C distances and smaller C−S2−C angles indicate that S2 has higher p-character than S1.

^{1}H NMR spectra of **3a**−**3e** in $CDCl_3$ are shown in Supporting Information, Figure S2. The downfield-shifted NH signals again suggested the presence of NH···S hydrogen bonds. The NH chemical shifts were observed in the order **3c** > **3b** > **3e** > **3d** > **3a**. For **3a**, the NH and 4-H signals were broadened in comparison with the other compounds. Because the 4-H proton is located in the neighborhood of the carbonyl group, the proton is deshielded by the π-electrons of the amide group depending on the torsion angle around the C13−N1 bond in Supporting Information, Figure S1. The broadened signal of **3a** was probably caused by the thermal rotational motion of the amide plane. The presence of an NH···S bond was established by IR spectroscopy under similar conditions to those shown in Supporting Information, Table S2. The strength of the NH···S hydrogen bond was evaluated by the reported method using the values of the corresponding disulfide, (S-2-RCONHC$_6$H$_4$)$_2$, in CH_2Cl_2.[13,17,24] The difference indicates the relative strength of the hydrogen bond. The order of strength was **3c** > **3b** > **3e** ≈ **3d** > **3a**, which was consistent with the ^{1}H NMR results. The strength of the NH···S hydrogen bond was dependent on the electron density of the sulfur atom, which was influenced by the neighboring atom or functional groups. In metal complexes, the nature of the metal ions or the other binding ligands, oxidation state, coordination number, and geometry also affect the strength.[14] In this case, the *i*-Pr group acted as an electron-donating group to sufficiently increase the electron density on sulfur to form a NH···S hydrogen bond.

The removal of the protecting isopropyl groups of **3a** and **3b** following air oxidation gave dibenzo[*c*,*g*][1,2,5,6]tetrathiocin derivatives, **4a** and **4b**, with two disulfide linkages. Attempted deprotection of **3c**−**3e** by the same method was unsuccessful, but another procedure gave positive results. Acylation of the amine that was prepared by the hydrolysis of **4a** gave **4c**−**4e**. ^{1}H NMR spectra of **4a**−**4c** revealed a mixture of *trans* and *cis* isomers, whereas **4d** and **4e** exhibited one set of peaks. This indicated that the bulky substituent prevented the formation of the *cis* isomer to avoid steric congestion. Because either isomer gives the same dithiolato ligand by reduction, separation of isomers was unnecessary in this step.

Synthesis of the Molybdenum Complexes. Monooxomolybdenum(IV) complexes were synthesized by a method similar to that previously reported.[20,24,25] The precursors of the ligands, **4a**−**4e**, were reacted with $(NEt_4)_2[Mo^{IV}O(S\text{-}4\text{-}ClC_6H_4)_4]$[29] in 1,2-dimethoxyethane (DME) or acetonitrile at ambient temperature. The reported method using $(NEt_4)[Mo^{V}O(SPh)_4]$ and NEt_4BH_4 effectively afforded the monooxomolybdenum(IV) complexes, but this reaction required excess water to avoid the formation of tris(dithiolene) derivatives.[24] Both methods gave the products, which were isolated as crystalline powders, in comparable yields. The reaction produced some byproducts caused by incomplete ligand-exchange reaction or the formation of dinuclear and unknown complexes. The byproducts were soluble in DME, therefore, removed by exhaustive washing, resulting in the low yields of the products. Unfortunately, many crystallization trials failed for our complexes. As described in the next section, **5a**−**5d** contained both *trans* and *cis* isomers, but **5e**, with extremely bulky substituents, was found to be a single isomer, most likely the *trans* isomer to avoid steric

dx.doi.org/10.1021/ic302149p | *Inorg. Chem.* 2013, 52, 381−394

hindrance. Both isomers reacted with Me_3NO to give a single isomer of **6a**−**6e**, as illustrated in Scheme 1.

Solution Structures of the Monooxomolybdenum(IV) Complexes. The aromatic regions of the ^{1}H NMR spectra of **5a**−**5e** in CD_3CN are shown in Figure 3. Peak assignments and

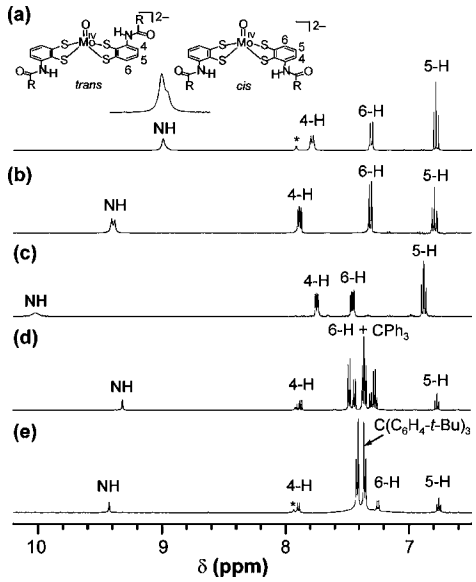

Figure 3. ^{1}H NMR spectra of (a) **5a**, (b) **5b**, (c) **5c**, (d) **5d**, and (e) **5e** in CD_3CN at 30 °C. The asterisk denotes DMF as a contaminant.

proposed structures of the two isomers are included. Two sets of peaks, assignable to the *trans* and *cis* isomers, were found for **5a**−**5d**. The chemical shift differences between the two isomers were smaller than those of the previously reported $(NE_4)_2[Mo^{IV}O(1,2\text{-}S\text{-}3\text{-}t\text{-}BuNHCOC_6H_3)_2]$.[25] The enlarged NH peak in **5a** indicates a 2:1 mixture of the isomers. The major peak is presumably the sterically favorable *trans* isomer. The signals of **5a** were slightly broader than those of the others, which suggests the presence of the thermal motion of the amide plane as found in **3a**. The most downfield-shifted NH peak of **5c** suggests the strongest NH···S hydrogen bond among these complexes, although solvation effects should be considered. ^{1}H NMR spectra revealed the presence of *trans* and *cis* isomers; however, the other spectra (IR, Raman) or redox potentials did not show distinct peaks for the two isomers. These results indicate that the difference between the two isomers is very small or indistinguishable; therefore, two isomers exhibit the same properties within the resolution of our measurements. The validity of this estimation was confirmed by the theoretical calculations described in the discussion.

IR and Resonance Raman Spectra. To evaluate the strength of the NH···S hydrogen bond, IR spectra in the solid state were obtained and listed in Table 1, with the values of the corresponding disulfides $(S\text{-}2\text{-}RCONHC_6H_4)_2$ in CH_2Cl_2. As described in previous papers, a large negative shift value, $\Delta\nu$(NH), indicates the presence of a strong NH···S hydrogen bond.[13,17,24] The estimated order of the strength of the hydrogen bonds was **5c** > **5b** > **5a** > **5e** ≈ **5d**. The obviously stronger NH···S of **5c** reasonably explains the downfield-shifted NH signal in the ^{1}H NMR spectrum. The $\Delta\nu$(NH) values (−50 to −89) of **5a**−**5d** were larger than those (−36 to −52) of the corresponding complexes $(NEt_4)_2[MoO\{S_2\text{-}3,6\text{-}(RCONH)_2C_6H_2\}_2]$ (R = CH_3, **7a**; *t*-Bu, **7b**; CF_3, **7c**; CPh_3, **7d**), with four NH···S hydrogen bonds, by about 1.2−1.8 times.[24] This fact suggests that the electron of the non-hydrogen-bonded thiolate was delocalized over the dithiolene moiety, increasing the electron density of the other thiolate and resulting in a stronger hydrogen bond. Such unsymmetrical electronic structures of these 3-acylaminobenzenedithiolates are of fundamental significance in the present study. The push−pull-like adjustment of these ligands should contribute to the stabilization of the unsymmetrical structure of the molybdenum complexes, as described below.

The NH···S hydrogen bond formed more effectively in the dioxomolybdenum(VI) complexes **6a**−**6e**. The order of hydrogen bond strength, **6c** > **6b** > **6a** > **6d** > **6e**, was similar to **5a**−**5e**. Because dioxomolybdenum(VI) complexes with four NH···S hydrogen bonds, $(NEt_4)_2[Mo^{VI}O_2\{S_2\text{-}3,6\text{-}(RCONH)_2C_6H_2\}_2]$,[24] were too unstable to be isolated, tungsten analogues were used as references. Substitution of molybdenum by tungsten resulted in comparable or weaker NH···S hydrogen bonds in monooxometal(IV) complexes, $(NEt_4)_2[M^{IV}O\{S_2\text{-}3,6\text{-}(RCONH)_2C_6H_2\}_2]$ (M = Mo, W). The differences between tungsten and molybdenum, $\Delta_{W-Mo}\nu$(NH), were 0 for R = CH_3 and 11 for R = *t*-Bu. In each dioxotungsten(VI) analogue, $(NEt_4)_2[W^{VI}O_2\{S_2\text{-}3,6\text{-}(RCONH)_2C_6H_2\}_2]$, two distinct ν(NH)s were observed and assigned to those at positions *trans* and *cis* to the terminal oxo ligand. The shifts from the disulfides, $\Delta\nu$(NH) values, were −12 and −66 for R = CH_3, and −24 and −65 for R = *t*-Bu. The larger negative values were ascribed to the stronger NH···S hydrogen bond at the *trans* position.[37] The $\Delta\nu$(NH) values for **6a** and **6b** were more negative than the tungsten analogues by 8

Table 1. IR Bands of ν(NH) (cm^{-1}) in the Molybdenum Complexes in the Solid State Compared with the Corresponding Disulfide, $(S\text{-}2\text{-}RCONHC_6H_4)_2$ in a CH_2Cl_2 Solution

		R	Mo complexes[a]	$(S\text{-}2\text{-}RCONHC_6H_4)_2$[b]	$\Delta\nu$(NH)
$Mo^{IV}O$	**5a**	CH_3	3321	3382	−61
	5b	*t*-Bu	3331	3397	−66
	5c	CF_3	3269	3358	−89
	5d	CPh_3	3291	3341	−50
	5e	$C(C_6H_4\text{-}4\text{-}t\text{-}Bu)_3$	3289	3342	−53
$Mo^{VI}O_2$	**6a**	CH_3	3308	3382	−74
	6b	*t*-Bu	3302	3397	−95
	6c	CF_3	3229	3358	−129
	6d	CPh_3	3272	3341	−69
	6e	$C(C_6H_4\text{-}4\text{-}t\text{-}Bu)_3$	3285	3342	−57

[a]Nujol. [b]In CH_2Cl_2 (10 mM).

dx.doi.org/10.1021/ic302149p | *Inorg. Chem.* 2013, 52, 381−394

and 30 cm^{-1}, respectively. The results clearly demonstrated that the unsymmetrical substitution effectively localized the negative charge on the hydrogen-bonded thiolate anion.

Resonance Raman and IR spectra of **5a**−**5e** in the solid state were measured, and ν(Mo═O)s are summarized in Table 2.

Table 2. Raman and IR Bands of Molybdenum Complexes in the Solid State

	ν(Mo═O)[a]/cm^{-1}	
$Mo^{IV}O$	Raman	IR
5a	910 (+8)	910 (+5)
5b	915 (+13)	914 (+9)
5c	914 (+12)	913 (+8)
5d	920 (+18)	917 (+12)
5e	911 (+9)	910 (+5)
8[b]	902	905
	Raman[c]	
$Mo^{VI}O_2$	ν_s(Mo═O)/cm^{-1}	ν_{as}(Mo═O)/cm^{-1}
6a	870 (+12)	840 (+11)
6b	873 (+15)	842 (+13)
6c	878 (+20)	844 (+15)
6d	868 (+10)	835 (+6)
6e	870 (+12)	839 (+10)
9[d]	858	829

[a]Differences from the value of $(NEt_4)_2[Mo^{IV}O(bdt)_2]$ (**8**) are shown in the parentheses. [b]Refs 23, 47. [c]Differences from the value of $(NEt_4)_2[Mo^{VI}O_2(bdt)_2]$ (**9**) are shown in the parentheses. [d]Ref 12.

To evaluate the contribution of the NH···S hydrogen bonds, the differences from the value of $(NEt_4)_2[Mo^{IV}O(bdt)_2]$ (**8**)[23,47] are also shown, parenthetically. All complexes showed higher ν(Mo═O) than that of **8**, where the order was **5d** > **5b** ≈ **5c** > **5e** ≈ **5a**. Each complex exhibited a weaker ν(Mo═O) in comparison with the corresponding $(NEt_4)_2[M^{IV}O\{S_2\text{-}3,6\text{-}(RCONH)_2C_6H_2\}_2]$ (**7a**−**7d**) with four NH···S hydrogen bonds, where ν(Mo═O)s were found at 914−928 cm^{-1}.[24] The individual hydrogen bonds of **5a**−**5d** were stronger than those of the corresponding **7a**−**7d**; however, the overall contributions did not surpass the combined power of the four hydrogen bonds in **7a**−**7d**. Dioxomolybdenum(VI) complexes **6a**−**6e** exhibited characteristic bands, that is, symmetric and asymmetric ν(Mo═O)s, ascribed to the *cis*-dioxo configuration. These values are listed in Table 2 together with the differences from those of $(NEt_4)_2[Mo^{VI}O_2(bdt)_2]$ (**9**).[12] The higher wavenumber shifts were 10−20 cm^{-1} and occurred in the order **6c** > **6b** > **6a** ≈ **6e** ≥ **6d**, which roughly agrees with the strength of the hydrogen bond.

Electrochemical Properties. Cyclic voltammograms of **5a** in DMF are shown in Figure 4, and the redox potentials of **5a**−**5e** and **8** are listed in Table 3. A quasi-reversible Mo(IV)/Mo(V) redox couple and irreversible oxidation to Mo(VI) species were observed as well-known redox behaviors for analogous complexes.[19,23,24] The redox potentials were found in the order **5c** > **5b** > **5a** > **5d** > **5e**, which was consistent with the strength of the NH···S hydrogen bonds. The positive shifts of **5a**−**5d** were smaller than the corresponding $(NEt_4)_2[MoO\{S_2\text{-}3,6\text{-}(RCONH)_2C_6H_2\}_2]$ (**7a**−**7d**), where the alphabetic notation follows **5a**−**5d**.[24] In the case of R = CF_3, $\Delta E_{1/2}$ values were +0.24 V for **6c** and +0.46 V for **7c**. When the number of the hydrogen bonds was halved from four to two, the $\Delta E_{1/2}$ value decreased by half. Such additivity, that is, a linear relationship between the positive shift of the redox potential and the number of NH···S hydrogen bonds, has been found for related compounds.[13,16,18]

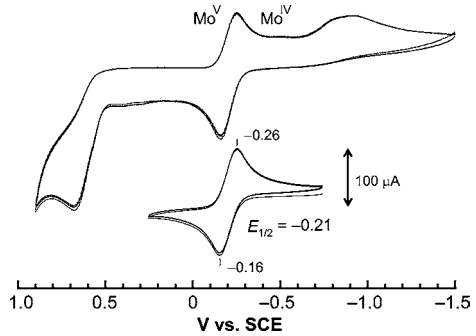

Figure 4. Cyclic voltammograms of $(NEt_4)_2[Mo^{IV}O(1,2\text{-}S_2\text{-}3\text{-}CH_3CONHC_6H_3)_2]$ (**5a**) in DMF. Two scans were obtained in the different ranges of the potential.

Table 3. Redox Potentials in DMF[a]

complex	$E_{1/2}$	$\Delta E_{1/2}$[b]
5a	−0.21	+0.17
5b	−0.19	+0.19
5c	−0.14	+0.24
5d	−0.24	+0.14
5e	−0.28	+0.10
8[c]	−0.38	

[a]$[Mo^{IV}O]$ = 2.5 mM. $[n\text{-}Bu_4NClO_4]$ = 0.1 M. Potentials are reported vs SCE at Pt working electrode. The scan rate was 100 mV/s. [b]The shifts from the value of $(NEt_4)_2[Mo^{IV}O(bdt)_2]$ (**8**). [c]Ref 47.

Absorption Spectra. UV−visible spectra of **5a**−**5e** and **6a**−**6e** in DMF are shown in Figure 5. The spectra of **5a** and **5b** were essentially identical and were identical to those of $(NEt_4)_2[Mo^{IV}O(bdt)_2]$ (**8**), except for a small shift and change in the absorbance.[23] The absorption band at ∼330 nm was ascribed to the ligand-to-metal charge-transfer (LMCT) band.[23] The peak maxima at 331 nm of **5a** and **5b** were equal to that of $(NEt_4)_2[Mo^{IV}O(tdt)_2]$ (tdt = 3,4-toluenedithiolato) rather than **8** (328 nm). This small red shift indicated that the acylamino group acts as a weak electron-donating group. The shape of each spectrum from **5a**−**5d** resembled the corresponding reported spectra for **7a**−**7d**.[24] The shape predominantly depended on the nature of the substituent, not on the number. The LMCT bands overlapped with the ligand absorptions; thus, the distinct maximum for **5a** was found as a shoulder peak in **7a**. The broad weak peaks at ∼450 nm were assignable to d−d bands. The similarity indicates the absence of significant geometrical changes in these complexes.[24]

Molybdenum(VI) complexes have d^0 configuration; thus, the lowest-energy absorptions at about 510−530 nm were assigned to LMCT bands. Previously, the excitation profiles revealed that the bands included both thiolate-to-Mo and oxo-to-Mo LMCT bands.[48] The higher-energy absorptions, that is, 300 nm < λ < 450 nm, were also more intense than in the case of **5a**−**5d**, and thus, they should be ascribed to LMCT bands. Consequently, the absorption bands of **6a**−**6e** were characteristic of dioxomolybdenum(VI) bis(dithiolate) complexes and proved the formation of the products.

Reduction of Trimethylamine *N*-oxide. Stoichiometric reactions between **5a**−**5e** and trimethylamine *N*-oxide in DMF were monitored by absorption spectroscopy. Observed rate

dx.doi.org/10.1021/ic302149p | *Inorg. Chem.* 2013, 52, 381−394

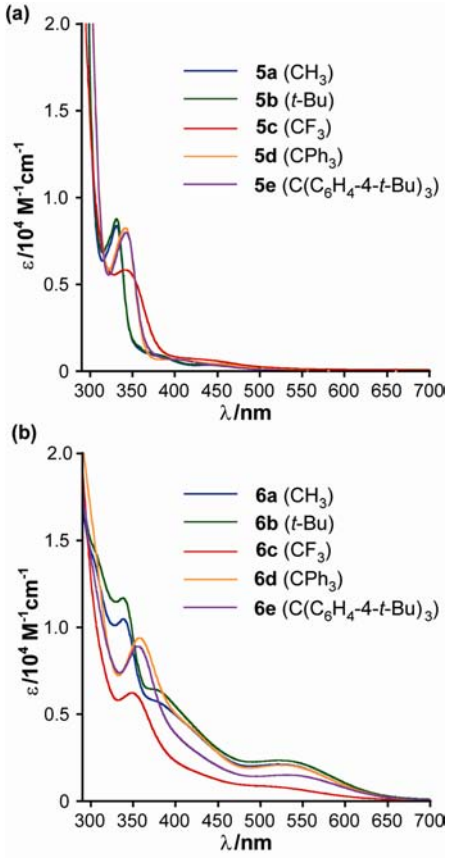

Figure 5. UV−visible spectra of (a) **5a**−**5e** and (b) **6a**−**6e** in DMF. Each substituent R is shown in the parentheses.

constants k_{obs} were obtained by pseudo-first-order kinetic analyses. The spectral change for the reaction of **5a** with 2 equivalents Me_3NO to give **6a** is shown in Figure 6. The absorption maximum at 525 nm due to the LMCT band of **6a** increased gradually. At the initial stage (up to 30% conversion), a logarithmic plot of the decrease in **5a** against the reaction time gave a linear correlation with the slope, $-k_{obs}$, as shown in the inset in Figure 6. In a similar manner, the rate constants were obtained for various Me_3NO concentrations (2−10 mM),

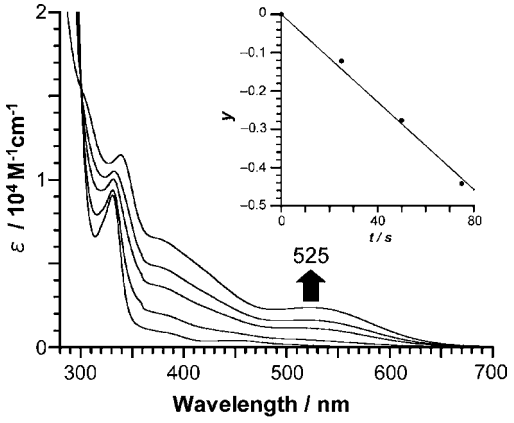

Figure 6. UV−visible spectral change of **5a** to **6a** on the stoichiometric reaction between **5a** and Me_3NO in DMF at 27 °C ($[Mo^{IV}O]$ = 1 mM, $[Me_3NO]$ = 2 mM). Pseudo-first order kinetics of **5a** to **6a** is shown in the inset, where the fitting line is $y = \ln(1 - [Mo^{VI}O_2]/[Mo^{IV}O]_0) = -k_{obs}\cdot t$ and $k_{obs} = 57 \times 10^{-4}$ s^{-1}.

which are summarized in Table 4 along with the data for related complexes.[24] The constants for **5d** and **5e** are almost equal

Table 4. Observed Initial Reaction Rate Constants (k_{obs}) in the Reaction between Monooxomolybdenum(IV) Complexes and Me_3NO in DMF at 27 °C

	k_{obs} (10^{-4}s^{-1})			
complex	$[Me_3NO]$ = 2 mM	$[Me_3NO]$ = 6 mM	$[Me_3NO]$ = 8 mM	$[Me_3NO]$ = 10 mM
5a	57 ± 9	248 ± 48	317 ± 79	377 ± 72
5b	77 ± 14	261 ± 69	420 ± 48	543 ± 24
5c	8 ± 3			9 ± 2
5d	25 ± 8	90 ± 26	158 ± 23	212 ± 43
5e	28 ± 3	97 ± 25		144 ± 35
7a[a]	49 ± 1	~140[b]		130 ± 1
7b[a]	3.3 ± 0.1			3.3 ± 0.1
7c[a]	35 ± 1			
7d[a]	260 ± 10			1700 ± 400
8[a]	5.4 ± 0.1			57 ± 4

[a]Ref 24. [b]The value was read from the graph in the literature.

within the experimental errors. The reaction rate constants k_{obs} were in the order **5b** > **5a** > **5d** ≈ **5e** > **5c**. This trend was similar to the strength of the NH···S hydrogen bonds, except for **5c**. The results were very different from **7a**−**7d**. These complicated trends were related to bulkiness or steric hindrance and the intermediates of the reaction. A comprehensive analysis and explanation are described, with theoretical calculations, in another section. The dependence of k_{obs} on the concentration of the substrate Me_3NO indicates that these reactions are essentially second-order, except for **5c** (Supporting Information, Figure S3). Second-order kinetics analysis gave reasonable results (Supporting Information, Figure S4). The second-order rate constants, k_2, were 4.1 ± 0.7 M^{-1} s^{-1} for **5a**, 6.7 ± 0.3 M^{-1} s^{-1} for **5b**, 2.1 ± 0.4 M^{-1} s^{-1} for **5d**, and 2.2 ± 0.4 M^{-1} s^{-1} for **5e**. The rate constant k_2 for **5a** was larger than that of **7a** (2.3 M^{-1} s^{-1}) with four NH···S hydrogen bonds.[37] Disparity in the reactivities between *trans* and *cis* isomers was hardly detectable. When a *trans*/*cis* mixture of **5c** was allowed to react with Me_3NO while being monitored by ^{1}H NMR spectroscopy, the *trans*/*cis* ratio was retained during the reaction.

Structures of the Dioxomolybdenum(VI) Complexes. ^{1}H NMR spectra of **6a**−**6e** in CD_3CN at 30 °C are shown in Figure 7. Each complex exhibited one set of peaks, suggesting the presence of a single isomer with equivalent ligands. According to the interpretation in the previous paper, it was reasonable that the NH···S hydrogen-bonded thiolates were located at the position *trans* to the oxo ligand, as illustrated in Figure 7.[25] This isomer is designated "**A**" in this paper. Another isomer with equivalent ligands is termed "**B**", where the hydrogen bond is *cis* to the oxo ligand, as shown in Supporting Information, Figure S7. Both isomers have a 2-fold axis through the bisected line of the O−Mo−O angle. A comparison of the ^{1}H NMR spectra for **5b** and **6b** is shown in Supporting Information, Figure S5. Two sets of peaks for the coordinated ligands in **5b** changed to one set of peaks in **6b**. The NH, 6-H, and *t*-Bu signals of **5b** were shifted upfield by 0.57, 0.47, and 0.17 ppm, respectively. IR spectra revealed that the NH···S hydrogen bond of **6b** was stronger than that of **5b**, as described above (Table 1). If the other contributions are ignored, the NH signal should be shifted downfield from **5b** to **6b**. Thus, the upfield shift must be caused by spatial shielding effects of the

dx.doi.org/10.1021/ic302149p | Inorg. Chem. 2013, 52, 381−394

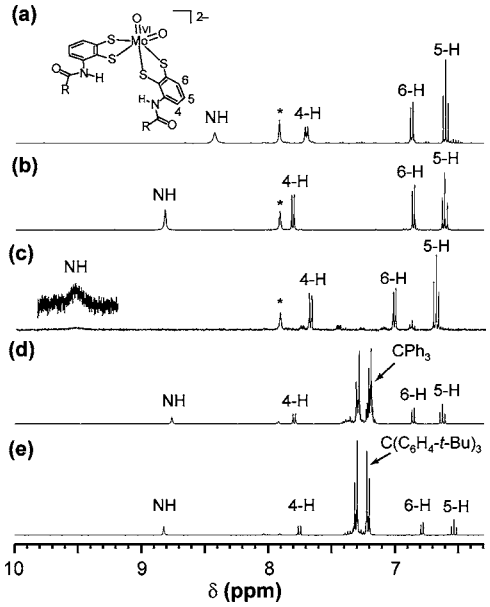

Figure 7. ^{1}H NMR spectra of (a) **6a**, (b) **6b**, (c) **6c**, (d) **6d**, and (e) **6e** in CD_3CN at 30 °C. An asterisk (*) indicates DMF as a contaminant.

delocalized π-electrons on the ligand. A similar situation was discussed previously.[25] Interligand interactions in **6b** are illustrated in Supporting Information, Figure S6. The *t*-Bu group was located over the benzene ring of the other ligand in the same molecule. The spatial proximity resulted in the observation of NOEs. The GOESY spectrum indicated that the *t*-Bu group was close to the 5- and 6-H protons by the favorable interligand orientation, while intraligand contacts were observed as intense signals (Supporting Information, Figure S6). These results demonstrated clearly that isomer **A** represented the unique configuration of **6a**−**6e**. The NH···S hydrogen bond must be situated at the position *trans* to the terminal oxo ligand.

DISCUSSION

Thermodynamic Stability of the Isomers for the $Mo^{IV}O$ and $Mo^{VI}O_2$ Complexes. ^{1}H NMR spectra revealed that each isolated **5a**−**5d** comprised a mixture of *trans* and *cis* isomers. The differences in the thermodynamic stabilities between the *trans* and *cis* isomers were estimated by theoretical calculations. Geometry optimizations were performed by DFT calculations, and the optimized structures of *trans* and *cis* isomers of **5b** are shown in Supporting Information, Figure S7. Selected geometric and electrostatic parameters are summarized in Supporting Information, Table S3 with the parameters for **8** as a reference. As two ligands are identical, only one set of parameters is shown for each complex. The hydrogen-bonded sulfur was designated S1, linked to C1, and the other was S2−C2. In the table, the Wiberg bond index and atom−atom overlap-weighted natural atomic orbital (NAO) bond order are shown to estimate the covalency of the bond. The bond index is approximately equal to the conventional bond order. The positive values of atom−atom overlap-weighted NAO bond order indicates a bonding character or attractive interaction between the two atoms. The length and strength of the NH···S hydrogen bonds of *trans*- and *cis*-**5b** were approximately the same. For either *trans*- or *cis*-**5b**, the Mo−S and Mo═O bonds were shorter than those of **8**. In each ligand, Mo−S2 was shorter than Mo−S1. The Mo−S1 bond of **5b** was apparently shorter than that of **8**; however, the bond order demonstrated that the bond was weakened by the NH···S hydrogen bond, while the Mo−S2 bond was strengthened. These values suggested that the NH···S hydrogen bond slightly weakens Mo−S1 by direct contact to decrease the electron density on sulfur and strengthens the neighboring Mo−S2 bond by electronic interaction via the benzene ring. This effect was observed in previous studies on $(NEt_4)_2[Mo^{IV}O(S_2\text{-}3\text{-}t\text{-}BuNHCOC_6H_3)_2]$ and was discussed using X-ray structures and DFT calculations.[25] The unsymmetrically localized negative charge on the hydrogen-bonded sulfur increases the positive charge on the Mo atom, which is consistent with the positive shift of the redox potentials of **5b**. The lower energy level of the HOMO in **5b** than that in **8** also agreed with the observed one-electron oxidation potentials of the molybdenum(IV) complexes. The shorter or stronger Mo═O bond means significant donation from the oxo group to the Mo ion, that is, a decrease in the electron density of the oxo ligand. The natural charge of O, therefore, appears slightly less negative. The difference in the calculated total energy between the *trans* and *cis* isomers was less than 0.1 kcal mol^{-1}. This minor difference agrees with the experimental observation of a 1:1 mixture of *trans*/*cis* isomers. The difference of the redox potentials between *trans*- and *cis*-**5b** was estimated from the energy level of HOMO listed in Supporting Information, Table S3. The calculated value is ∼3 mV, which is negligibly small and experimentally undetectable. The estimated differences of the vibrational energy between *trans*- and *cis*-**5b** were ∼1.7 cm^{-1} for ν(NH) and ∼0.3 cm^{-1} for ν(Mo═O) from the frequency calculations. These values are too small to detect each signal separately in broad IR and Raman spectra.

The dioxomolybdenum(VI) complexes **6a**−**6e** were present in solution as the unique isomer **A**, where the hydrogen-bonded thiolate was *trans* to the terminal oxo ligand, as estimated from the spectroscopic analysis. To confirm this conclusion, the optimized structures of isomers **A** and **B** for **6b** were calculated. The structures of **6b**-**A** and **6b**-**B**, in addition to **9**, are shown in Supporting Information, Figure S7. The geometric and electrostatic parameters are summarized in Supporting Information, Table S4. For these complexes, the sulfur atom at the position *trans* to oxo ligand is labeled S1, connected to C1, and the other is S2. The total energy of **6b**-**A** was calculated to be less than that of **6b**-**B** by approximately 5.38 kcal mol^{-1}. These results demonstrated clearly that **6b**-**A** is a unique isomer, although the difference in the calculated energies was not very large. This difference was comparable to the previously reported value.[25] Unlike *trans*-**5b** and *cis*-**5b**, the two isomers showed significant differences with each other. The NH···S hydrogen bond distance of **6b**-**A** was shorter than that of **6b**-**B**. Both the bond index and bond order of **6b**-**A** clearly indicated an increase in covalency in comparison with that of the corresponding monooxomolybdenum(IV) complex, **5b**. These results were in good agreement with the values of ν(NH) in the IR spectra. The Mo═O bond of **6b**-**A** was significantly shorter than those of **6b**-**B** and **9**, which was consistent with the Raman spectral observations. In **6b**-**A**, Mo−S1 bond was obviously longer than Mo−S2 by 0.2256 Å. The long Mo−S1 bond localizes the negative charge of the thiolate anion on the sulfur atom (calculated natural charge is −0.25738), which is favorable for the formation of the NH···S hydrogen bond. Conversely, the hydrogen bond stabilizes the localized electron on sulfur and enables the thiolate to maintain the

dx.doi.org/10.1021/ic302149p | Inorg. Chem. 2013, 52, 381−394

extraordinarily long Mo−S1 bond. On the other hand, the short Mo−S2 indicates significant electron-donation from S2 to Mo, resulting in the lower negative natural charge on S2 (−0.12336). In **6b-B**, the difference between Mo−S1 and Mo−S2 was smaller than those in **6b-A** and **9**. The originally localized negative charge on S1 was distributed between S1 and S2 as an averaged charge. The configuration of **B** has the opposite effect on the stabilization of **6b**.

Relation between the Strength of NH···S Hydrogen Bonds and the Redox Potential. NH···S hydrogen bonds are known to shift redox potentials in a positive manner. The relationship between the strength of the hydrogen bond and the positive shift has been analyzed qualitatively.[13,16,18,19,24] A quantitative analysis is presented here. Using the data in Tables 1 and 3, $\Delta E_{1/2}$ values were plotted against $-\Delta\nu$(NH), where the values for **8** were assumed as $\Delta\nu$(NH) = $\Delta E_{1/2}$ = 0 (i.e., the origin) (Figure 8a). The plot clearly indicates a strong

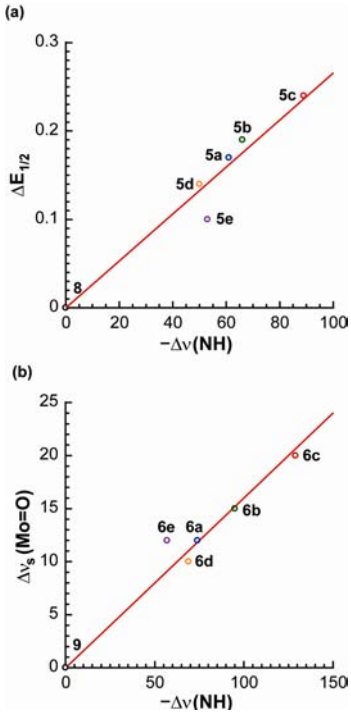

Figure 8. Correlation (a) between $\Delta\nu$(NH) and $\Delta E_{1/2}$ in the monooxomolybdenum(IV) complexes and (b) between $\Delta\nu$(NH) and $\Delta\nu_s$(Mo═O) in the dioxomolybdenum(VI) complexes. The original data are shown in Tables 1−3.

correlation, with r^2 = 0.94. The plot of **5e** deviated slightly from the fitting line. Complex **5e** has extremely bulky and hydrophobic $(4\text{-}t\text{-BuC}_6H_4)_3C$ groups. Generally, the negative shift of the redox potential in a solvent with a lower dielectric constant is known both theoretically and experimentally.[49−51] Our results suggest that the bulky, hydrophobic substituent partially masks the molybdenum center and creates a hydrophobic environment with a low dielectric constant.

Relation between the Strength of NH···S Hydrogen Bonds and Mo^{VI}═O Bonds. The contribution of the NH···S hydrogen bond to the Mo═O bond at the *trans* position is essentially the same as that described in the previous paper.[25] This is explained by the so-called "*trans* influence". O and S atoms, situated *trans* to one another, donate competitively to the Mo center in such dioxomolybdenum(VI) bis(dithiolate) complexes. Electron-rich thiolate is an intrinsically strong donor that interferes with donation by the oxo ligand to the molybdenum center. When the thiolate is hydrogen-bonded by an amide NH, its donating ability is decreased, ultimately as in the case of thioketone. This effect results in a strong Mo═O bond.

In this paper, the contributions of the NH···S hydrogen bond were evaluated using substituent effects. The strength of the NH···S hydrogen bond was in the order **6c** > **6b** > **6a** > **6d** > **6e**, estimated by $\Delta\nu$(NH) in the IR spectra. The strength of the Mo═O bond was in the order **6c** > **6b** > **6a** > **6e** ≈ **6d**, according to $\Delta\nu_s$(Mo═O) in the Raman spectra. The difference in ν_s(Mo═O) between **6d** and **6e** was about 2 cm^{-1}. The peaks were broad and noisy, and the resolution was 1−2 cm^{-1}; thus, they were approximately the same or within experimental error. A plot of $\Delta\nu_s$(Mo═O) values versus $\Delta\nu$(NH) for **6a**−**6e** is shown in Figure 8b, where the plot for **9** is placed at the origin, assuming ν_s(Mo═O) = $\Delta\nu$(NH) = 0. A strong correlation (r^2 = 0.96) was clearly demonstrated. The plot of **6e** deviated the most from the fitting line. As mentioned above, this deviation includes experimental error, and thus, a strict evaluation is difficult; however, another factor may possibly apply. The two extremely bulky substituents of **6e** are close to each other in the unique isomer **A**. Steric interactions probably result in a slight deformation from the original geometry, which must perturb the *trans* influence.

Reaction Mechanism for the Reduction of Me_3NO. For the reduction of Me_3NO by monooxomolybdenum(IV) complexes, two reaction mechanisms have been proposed, depending on the substituents.[23,24] In the traditional mechanism, Me_3NO first attacks Mo at the position *trans* to the oxo ligand to give an intermediate Me_3NO adduct. The $ONMe_3$ ligand moves to the *cis* position through a *trans*−*cis* rearrangement, accompanied by dissociation of the O−N bond to afford a *cis*-dioxomolybdenum(VI) complex. If the substituent is bulky or the intermediate is stabilized, the *trans*−*cis* rearrangement is the rate-determining step at high concentrations of Me_3NO. The reaction essentially obeys second-order kinetics; however, the apparent reaction rate reaches a maximum at high concentrations of Me_3NO when the substituent is bulky, such as Ph_3Si[23] or *t*-BuCONH.[24] This saturation of the reaction rate against the concentration of substrate is reminiscent of Michaelis−Menten kinetics, which are usually observed in enzymatic reactions. The reaction of **7a**, with relatively small CH_3CONH groups, also showed such saturation when [Me_3NO] > 6 mM.[24] In the case of **7d**, with four extraordinarily bulky Ph_3CCONH groups, the *trans*−*cis* rearrangement hardly occurred. Instead, the direct *cis* attack of Me_3NO proceeded. This is the alternative mechanism reported in the previous paper.[24] The bulky substituent groups induced a deformation of the $MoOS_4$ core and provided a vacant site at the *cis* position for the attack of Me_3NO, resulting in the remarkably fast reaction..

In the cases of **5d** and **5e**, very fast reactions (as in **7d**) were not observed (Table 4). Reduction of the number of the substituent groups from four to two probably enabled the *trans*−*cis* rearrangement. Interestingly, **5c** displayed saturation of k_{obs}, although rearrangement seemed to be sterically possible. These reactions were considered to proceed by the traditional mechanism, which included the attack of Me_3NO at the position *trans* to the oxo ligand followed by *trans*−*cis* rearrangement. To estimate the reaction mechanism, optimized structures of the putative intermediates were obtained by DFT

dx.doi.org/10.1021/ic302149p | *Inorg. Chem.* 2013, 52, 381−394

calculations. The structures of the Me_3NO-adducts of *trans*-**5b**, *cis*-**5b**, and **7b** are shown in Supporting Information, Figure S8. The geometrical parameters for these compounds, as well as the related adducts of **8** and **5c**, are listed in Supporting Information, Table S5. A comparison of monooxomolybdenum(IV) complexes (Supporting Information, Table S3) with the corresponding Me_3NO-adducts (Supporting Information, Table S5) showed that the Mo═O bond was shortened and the Mo−S bonds were elongated by the approach of Me_3NO, which resulted in a slightly distorted octahedral geometry of the Me_3NO-adducts. The molybdenum ion was deviated from the S_4 plane to form the square pyramidal geometry of the $MoOS_4$ core. The $ONMe_3$ ligand weakly coordinated to the molybdenum center with a Mo−O bond longer than 2.4 Å. The O═Mo−O bonds were approximately linear (about 174 or 175°). The Mo−O−N angles were bent at an angle of about 136−138°. Generally, the M−O−N (M: metal) bonds found in transition metal complexes[52,53] and organometallic aluminum complexes[54] are bent with an angle of about 120−130°. However, a weak Ba−O contact found in $[(Me_3NO)_2Ba_2Cu_4(OCMe_2CF_3)_8]$ resulted in an approximately linear Ba−O−N angle (~175°).[55] The optimized structures demonstrated that the Mo−$ONMe_3$ interaction was a weak, but stable, coordinate bond. The O═Mo−O bond was slightly bent toward the S2 atom, and the Mo−O−N angle was bent to the opposite side, that is, toward S4. The O═Mo−O−N connection was arranged in a zigzag pattern. The Me_3N moiety was located in the vicinity of S4 to avoid steric congestion with the bulky substituent. Except for *cis*-**5b**-$ONMe_3$, the shortest Mo−S bond was Mo−S2 and the longest was Mo−S4. The angle of O═Mo−S2 was the widest, and that of O═Mo−S4 was the narrowest. The relationship between the Mo−S distance and the O═Mo−S angle has been discussed for the monooxomolybdenum(V) tetrakis(arenethiolate) complex with distorted geometry between square-pyramidal and trigonal-bipyramidal.[19] A similar tendency was found in the optimized structure of *trans*-**5b** (Supporting Information, Table S3). As mentioned above, the hydrogen bond stabilizes the long Mo−S bond. For *trans*-**5b**-$ONMe_3$ and **5c**-$ONMe_3$, the longest Mo−S4 bond did not have an adjacent hydrogen bond, which probably caused an unstable Mo−S bond between the electron-rich S and electron-deficient Mo. The electron-deficient molybdenum was stabilized by the strongest Mo−S2 bond at the *trans* position. In the case of *cis*-**5b**-$ONMe_3$, the hydrogen-bonded Mo−S2 bond was *trans* to the Mo−S4 bond. The relatively weak donor S2 could not effectively stabilize the Mo−S4 bond via the molybdenum ion as described for *trans*-**5b**-$ONMe_3$. Instead of the interligand interaction, the distortion of the geometry was reduced, and the localized electron density was delocalized via the intraligand path. The distortion of the intermediates and the open space between the substituent groups of *trans*- and *cis*-**5b**-$ONMe_3$ promote the preferable motion toward *trans*−*cis* rearrangement. A proposed mechanism for the reduction of Me_3NO by **5a**−**5e**, including the *trans*−*cis* rearrangement, is given in Figure 9. Because there was no significant difference between the total energy of *trans*- and *cis*-**5b**-$ONMe_3$, as well as the ^1H NMR observation of the retention of the *trans*/*cis* ratio during the reaction, the two pathways are comparable. The arrows indicate the motion of the moiety and the rearrangement occurs successively, in the order of the encircled numbers. In the *trans* isomer, the weakest Mo−S bond rotationally moves to the left side to open the space at the opposite side. Next, the Me_3NO

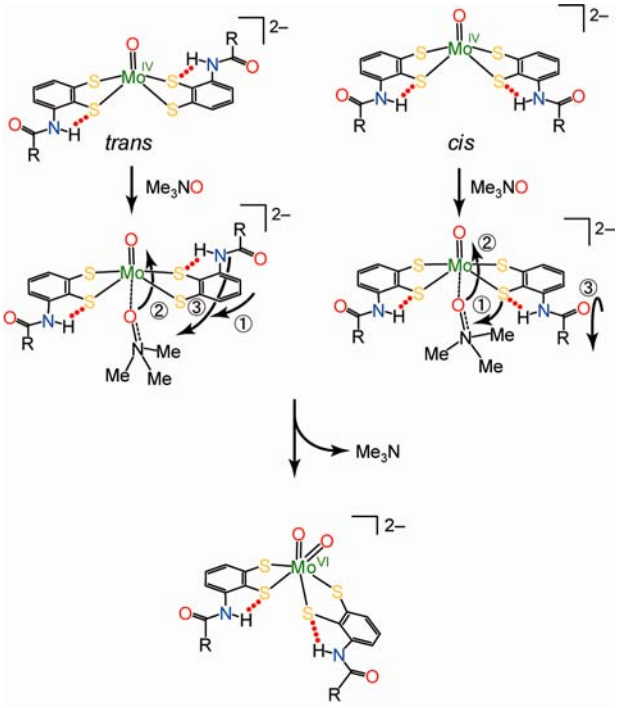

Figure 9. Proposed mechanism for the reduction of Me_3NO by **5a**−**5e** via *trans*−*cis* rearrangement. The intermediates are stabilized by the NH···S hydrogen bond, especially for **5c** (R = CF_3).

moiety rises at the back and across the open space. Simultaneously, the right ligand rotates clockwise around the Mo−S bond at the front to move the hydrogen-bonded thiolate to the bottom. The *trans*−*cis* rearrangement involves an intramolecular two electron transfer from Mo^{IV} to $ONMe_3$, accompanying the formation of a Mo^{VI}═O bond and the release of NMe_3. The widest O═Mo−S angle and the shortest Mo−S bond on the far side of the left ligand is retained during the rearrangement and becomes the widest O═Mo−S and the shorter Mo−S of the corresponding dioxomolybdenum(VI) complex. For the *cis* isomer, the mechanism is similar to that for the *trans* isomer, except that the final rotation is counterclockwise. In this case, the three steps probably proceed in a concerted fashion.

In the intermediates, the NH···S hydrogen bonds obviously stabilized both Mo═O and Mo−O(NMe_3) bonds. In particular, the bonds of **7b**-$ONMe_3$ and **5c**-$ONMe_3$ were effectively shortened (Supporting Information, Table S5). These data indicate that both the number and the strength of the NH···S hydrogen bonds contributed to the stabilization of the intermediates. The space-filling model of **7b**-$ONMe_3$ revealed that steric congestion prevented or retarded the rotation of the ligand that is required for rearrangement (Supporting Information, Figure S8c). These results reasonably explain the small observed rate constant (k_{obs} = 3.3 ± 0.1 s^{-1}; $[Me_3NO] \geq 2$ mM) for **7b**. A significantly strong hydrogen bond sufficiently stabilized the intermediate. In the case of **5c**, the value of k_{obs} was saturated at about 9 s^{-1} for $[Me_3NO] \geq 2$ mM. The rearrangement of **5c**-$ONMe_3$ was retarded by the strong hydrogen bond in spite of apparently sufficient space available for the rearrangement.

The alternative *cis*-attack mechanism was proposed for the reaction of Me_3NO and **7d** (with four Ph_3CCONH groups) in the previous paper.[24] The mechanism is reconsidered here

dx.doi.org/10.1021/ic302149p | *Inorg. Chem.* 2013, 52, 381−394

using DFT calculations. To limit computational costs, a complex without any substituents, $[MoO(bdt)_2]^{2-}$ (**8**), was used in the calculations. When the constraint of Mo−O(NMe_3) distance was not used, the optimization converged to the starting model or the product, $[MoO_2(bdt)_2]^{2-}$ (**9**) and Me_3N, depending on the starting model. The optimized structures are shown in Supporting Information, Figure S9, with the fixed distance of Mo···O. From a distance of ∼4 Å and diagonally from above, molecular Me_3NO was approached step-by-step to the molybdenum center. In the range of 4−2.1 Å, the final structure was the Me_3NO-adduct. In accordance with the approach of Me_3NO, the MoO_2S_4 core was distorted to octahedral geometry and the Mo−S distance *trans* to the oxo ligand was elongated. The positively charged Me_3N moiety tended to be drawn by the basic terminal oxo ligand. At Mo···O = 2.1 Å, the N−O−Mo angle was about 128°, which agrees with the reported values for transition metal complexes.[52,53] Within 1.8 Å of Mo−O contact, the structure converged to the dioxomolybdenum(VI) complex and Me_3N. In the range of 1.9−2.0 Å, the construct could not converge to a suitable structure. The total energy of the optimized structure increased with the approach of Me_3NO and dropped immediately upon cleavage of the O−N bond. These results suggest that the *cis* attack does not pass through a metastable intermediate such as a Me_3NO-adduct. The approach of Me_3NO and the cleavage of the N−O bond probably occur simultaneously, with concomitant formation of the dioxomolybdenum(VI) complex.

CONCLUSIONS

The monooxomolybdenum(IV) and dioxomolybdenum(VI) 3-acylaminobenzenedithiolate complexes having two intramolecular NH···S hydrogen bonds clearly demonstrated the contributions of NH···S hydrogen bonds to the properties and the reactivities of the complexes. The reactivities of the *trans* and *cis* isomers of the monooxomolybdenum(IV) complexes were essentially identical. Each dioxomolybdenum(VI) complex was found as a unique isomer where the hydrogen-bonded thiolate was *trans* to the terminal oxo ligand. Reduction of the number of the substituent groups from four to two successfully excluded the influence of steric factors and resulted in a good correlation between the strength of the hydrogen bond and the strength of Mo═O or the redox potential. The contribution from the substituents followed the order CF_3 > *t*-Bu > CH_3 > CPh_3 > $C(C_6H_4$-4-*t*-Bu$)_3$ for Mo(VI) and CF_3 > *t*-Bu > CH_3 > $C(C_6H_4$-4-*t*-Bu$)_3$ ≈ CPh_3 for Mo(IV). Rate constants followed approximately the same order, except for CF_3: *t*-Bu > CH_3 > CPh_3 ≈ $C(C_6H_4$-4-*t*-Bu$)_3$ ≫ CF_3. These data indicate that the strong NH···S hydrogen bond in **5c** (R = CF_3) effectively stabilized the intermediate and retarded the *trans*−*cis* rearrangement in the proposed mechanism. DFT calculations supported this consideration.

Consequently, the present data clearly demonstrate the contribution of the NH···S hydrogen bonds to the properties and the reactivities of the molybdoenzyme models, and suggest that the hydrogen bond is one of the important factors in the fine and delicate tuning of the reactivity of metalloenzymes in biological systems.

ASSOCIATED CONTENT

Supporting Information

X-ray crystallographic data for **1**, **3a**, **3b**, and **3d** in CIF format, crystallographic data (Table S1), molecular structures (Figure S1), proposed mechanism for **1** (Scheme S1), ^{1}H NMR (Figure S2) and IR (Table S2) spectra of **3a**−**3e**, dependence of k_{obs} on [Me_3NO] (Figure S3), second order kinetics for the reaction from **5a** to **6a** (Figure S4), ^{1}H NMR spectra of **5b** and **6b** (Figure S5), GOESY spectrum of **6b** (Figure S6), optimized structures for **5b**, **6b** (Figure S7) and geometrical parameters (Tables S3, S4), optimized structures of intermediates (Figures S8, S9) and their geometrical parameters (Table S5). This material is available free of charge via the Internet at http://pubs.acs.org.

AUTHOR INFORMATION

Corresponding Author

*E-mail: tokamura@chem.sci.osaka-u.ac.jp.

Notes

The authors declare no competing financial interest.

ACKNOWLEDGMENTS

This work was supported by JSPS KAKENHI Grant Number 23655049.

REFERENCES

(1) Hill, R. *Chem. Rev.* **1996**, *96*, 2757−2816.
(2) Pushie, M. J.; George, G. N. *Coord. Chem. Rev.* **2011**, *255*, 1055−1084.
(3) Messerschmidt, A., Huber, R., Poulos, T., Wieghardt, K., Eds.; *Handbook of Metalloproteins*; John Wiley & Sons, Ltd: Chichester, U.K., 2001; Vol. *2*.
(4) Enemark, J. H.; Cooney, J. J. A.; Wang, J.-J.; Holm, R. H. *Chem. Rev.* **2004**, *104*, 1175−1200.
(5) Holm, R. H.; Solomon, E. I.; Majumdar, A.; Tenderholt, A. *Coord. Chem. Rev.* **2011**, *255*, 993−1015.
(6) Ng, V. W. L.; Taylor, M. K.; Young, C. G. *Inorg. Chem.* **2012**, *51*, 3202−3211.
(7) Smith, P. D.; Millar, A. J.; Young, C. G.; Ghosh, M.; Basu, P. *J. Am. Chem. Soc.* **2000**, *122*, 9298−9299.
(8) Stiefel, E. I., Ed.; *Dithiolene Chemistry Synthesis, Properties, and Applications*; John Wiley & Sons, Inc.: Hoboken, NJ, 2004; Vol. *52*.
(9) Sugimoto, H.; Tsukube, H. *Chem. Soc. Rev.* **2008**, *37*, 2609−2619.
(10) Yoshinaga, N.; Ueyama, N.; Okamura, T.; Nakamura, A. *Chem. Lett.* **1990**, *19*, 1655−1656.
(11) Ueyama, N.; Yoshinaga, N.; Okamura, T.; Zaima, H.; Nakamura, A. *J. Mol. Catal.* **1991**, *64*, 247−256.
(12) Ueyama, N.; Oku, H.; Kondo, M.; Okamura, T.; Yoshinaga, N.; Nakamura, A. *Inorg. Chem.* **1996**, *35*, 643−650.
(13) Okamura, T.; Takamizawa, S.; Ueyama, N.; Nakamura, A. *Inorg. Chem.* **1998**, *37*, 18−28.
(14) Ueyama, N.; Okamura, T. In *Organometallic Conjugation*; Nakamura, A., Ueyama, N., Yamaguchi, K., Eds.; Kodansha: Tokyo, Japan, 2002; pp 265−306.
(15) Ueyama, N.; Okamura, T.; Nakamura, A. *J. Chem.Soc., Chem. Commun.* **1992**, 1019−1020.
(16) Ueyama, N.; Yamada, Y.; Okamura, T.; Kimura, S.; Nakamura, A. *Inorg. Chem.* **1996**, *35*, 6473−6484.
(17) Ueyama, N.; Nishikawa, N.; Yamada, Y.; Okamura, T.; Nakamura, A. *J. Am. Chem. Soc.* **1996**, *118*, 12826−12827.
(18) Ueyama, N.; Nishikawa, N.; Yamada, Y.; Okamura, T.; Oka, S.; Sakurai, H.; Nakamura, A. *Inorg. Chem.* **1998**, *37*, 2415−2421.
(19) Ueyama, N.; Okamura, T.; Nakamura, A. *J. Am. Chem. Soc.* **1992**, *114*, 8129−8137.
(20) Okamura, T.; Taniuchi, K.; Lee, K.; Yamamoto, H.; Ueyama, N.; Nakamura, A. *Inorg. Chem.* **2006**, *45*, 9374−9380.
(21) Okamura, T.; Ueyama, N.; Nakamura, A.; Ainscough, E. W.; Brodie, A. M.; Waters, J. M. *J. Chem.Soc., Chem. Commun.* **1993**, 1658−1659.
(22) Baba, K.; Okamura, T.; Yamamoto, H.; Yamamoto, T.; Ueyama, N. *Inorg. Chem.* **2008**, *47*, 2837−2848.

(23) Oku, H.; Ueyama, N.; Kondo, M.; Nakamura, A. *Inorg. Chem.* **1994**, *33*, 209−216.
(24) Baba, K.; Okamura, T.; Suzuki, C.; Yamamoto, H.; Yamamoto, T.; Ohama, M.; Ueyama, N. *Inorg. Chem.* **2006**, *45*, 884−901.
(25) Okamura, T.; Tatsumi, M.; Omi, Y.; Yamamoto, H.; Onitsuka, K. *Inorg. Chem.* **2012**, *51*, 11688−11697.
(26) Gibson, H. W.; Lee, S.-H.; Engen, P. T.; Lecavalier, P.; Sze, J.; Shen, Y. X.; Bheda, M. *J. Org. Chem.* **1993**, *58*, 3748−3756.
(27) Hahn., F. E.; Seidel., W. W. *Angew. Chem., Int. Ed. Engl.* **1995**, *34*, 2700−2703.
(28) Boyd, I. W.; Dabce, I. G.; Murray, K. S.; Wedd, A. G. *Aust. J. Chem.* **1978**, *31*, 279−284.
(29) Kondo, M.; Ueyama, N.; Fukuyama, K.; Nakamura, A. *Bull. Chem. Soc. Jpn.* **1993**, *66*, 1391−1396.
(30) Marinescu, L.; Thinggaard, J.; Thomsen, I. B.; Bols, M. *J. Org. Chem.* **2003**, *68*, 9453−9455.
(31) Ueyama, N.; Okamura, T.; Yamada, Y.; Nakamura, A. *J. Org. Chem.* **1995**, *60*, 4893−4899.
(32) Altomare, A.; Burla, M. C.; Camalli, M.; Cascarano, M.; Giacovazzo, C.; Guagliardi, A.; Polidori, G. *J. Appl. Crystallogr.* **1994**, *27*, 435.
(33) Sheldrick, G. M. *Acta Crystallogr.* **2008**, *A64*, 112−122.
(34) Frisch, M. J.; Trucks, G. W.; Schlegel, H. B.; Scuseria, G. E.; Robb, M. A.; Cheeseman, J. R.; Montgomery, J. A., Jr.; Vreven, T.; Kudin, K. N.; Burant, J. C.; Millam, J. M.; Iyengar, S. S.; Tomasi, J.; Barone, V.; Mennucci, B.; Cossi, M.; Scalmani, G.; Rega, N.; Petersson, G. A.; Nakatsuji, H.; Hada, M.; Ehara, M.; Toyota, K.; Fukuda, R.; Hasegawa, J.; Ishida, M.; Nakajima, T.; Honda, Y.; Kitao, O.; Nakai, H.; Klene, M.; Li, X.; Knox, J. E.; Hratchian, H. P.; Cross, J. B.; Adamo, C.; Jaramillo, J.; Gomperts, R.; Stratmann, R. E.; Yazyev, O.; Austin, A. J.; Cammi, R.; Pomelli, C.; Ochterski, J. W.; Ayala, P. Y.; Morokuma, K.; Voth, G. A.; Salvador, P.; Dannenberg, J. J.; Zakrzewski, V. G.; Dapprich, S.; Daniels, A. D.; Strain, M. C.; Farkas, O.; Malick, D. K.; Rabuck, A. D.; Raghavachari, K.; Foresman, J. B.; Ortiz, J. V.; Cui, Q.; Baboul, A. G.; Clifford, S.; Cioslowski, J.; Stefanov, B. B.; Liu, G.; Liashenko, A.; Piskorz, P.; Komaromi, I.; Martin, R. L.; Fox, D. J.; Keith, T.; Al-Laham, M. A.; Peng, C. Y. ; Nanayakkara, A.; Challacombe, M.; Gill, P. M. W.; Johnson, B.; Chen, W.; Wong, M. W.; Gonzalez, C.; Pople, J. A. *Gaussian03*, Revision E.01; Gaussian, Inc.: Pittsburgh, PA, 2004.
(35) Huzinaga, S., Ed.; *Gaussian Basis Sets for Molecular Calculations*; Elsevier: Amsterdam, The Netherlands, 1984.
(36) Yamanaka, S.; Kawamura, T.; Noro, T.; Yamaguchi, K. *J. Mol. Struct.* **1994**, *310*, 185−196.
(37) Baba, K.; Okamura, T.; Yamamoto, H.; Yamamoto, T.; Ohama, M.; Ueyama, N. *Inorg. Chem.* **2006**, *45*, 8365−8371.
(38) Hall, D. W.; Richards, J. H. *J. Org. Chem.* **1963**, *28*, 1549−1554.
(39) Newkome, G. R.; Gross, J.; Patri, K. *J. Org. Chem.* **1997**, *62*, 3013−3014.
(40) Okamura, T.; Iwamura, T.; Nozaki, K.; Ohno, T.; Yamamoto, H.; Ueyama, N. *Mol. Cryst. Liq. Cryst.* **2002**, *379*, 431−436.
(41) Lieber, E.; R., L. M., Jr.; Rao, C. N. R. *Chem. Rev.* **1965**, *65*, 377−384.
(42) Galeazzi, R.; Geremia, S.; Mobbili, G.; Orena, M. *Tetrahedron: Asymmetry* **1996**, *7*, 3573−3584.
(43) Krow, G. R.; Huang, Q.; Lin, G.; Centafont, R. A.; Thomas, A. M.; Gandla, D.; DeBrosse, C.; Carroll, P. J. *J. Org. Chem.* **2006**, *71*, 2090−2098.
(44) Fahr, E.; Neumann, L. *Angew. Chem., Int. Ed. Engl.* **1965**, *4*, 595.
(45) Yamaguchi, S.; Uchiuzoh, Y.; Sanada, K. *J. Heterocycl. Chem.* **1995**, *32*, 419−423.
(46) Liao, Y.; Venhuis, B. J.; Rodenhuis, N.; Timmerman, W.; Wikström, H. *J. Med. Chem.* **1999**, *42*, 2235−2244.
(47) Boyde, S.; Ellis, S. R.; Garner, C. D.; Clegg, W. *J. Chem. Soc., Chem. Commun.* **1986**, 1541−1543.
(48) Oku, H.; Ueyama, N.; Nakamura, A. *Inorg. Chem.* **1995**, *34*, 3667−3676.
(49) Kassner, R. J.; Yang, W. *J. Am. Chem. Soc.* **1977**, *99*, 4351−4355.
(50) Ueyama, N.; Terakawa, T.; Nakata, M.; Nakamura, A. *J. Am. Chem. Soc.* **1983**, *1983*, 7098−7102.
(51) Ohno, R.; Ueyama, N.; Nakamura, A. *Inorg. Chim. Acta* **1990**, *169*, 253−255.
(52) Nubel, P. O.; Wilson, S. R.; Brown, T. L. *Organometallics* **1983**, *2*, 515−525.
(53) Jin, S.; Nieuwenhuyzen, M.; Wilkins, C. J. *J. Chem. Soc., Dalton Trans.* **1992**, 2071−2078.
(54) Kai, Y.; Yasuoka, N.; Kasai, N.; Kakudo, M. *Bull. Chem. Soc. Jpn.* **1972**, *45*, 3388−3396.
(55) Borup, B.; Streib, W. E.; Caulton, K. G. *Inorg. Chem.* **1997**, *36*, 5058−5063.